Discontinuous Galerkin solutions of the Boltzmann equation: spectral collocation and moment methods

by

R. Loek Van Heyningen

Submitted to the Center for Computational Science and Engineering
in partial fulfillment of the requirements for the degree of

Master of Science in Computational Science and Engineering

at the

MASSACHUSETTS INSTITUTE OF TECHNOLOGY

June 2021

Author .....
Center for Computational Science and Engineering
May 21, 2021

Certified by .....
Jaime Peraire
H.N. Slater Professor of Aeronautics and Astronautics
Thesis Supervisor

Certified by .....
Ngoc-Cuong Nguyen
Principal Research Scientist
Thesis Supervisor

Accepted by .....
Youssef Marzouk
Professor of Aeronautics and Astronautics
Co-director, Center for Computational Science and Engineering

Discontinuous Galerkin solutions of the Boltzmann equation: spectral collocation and moment methods

by

R. Loek Van Heyningen

Submitted to the Center for Computational Science and Engineering
on May 21, 2021, in partial fulfillment of the
requirements for the degree of
Master of Science in Computational Science and Engineering

Abstract

This thesis explores the ability of the discontinuous Galerkin (DG) method to numerically solve the Boltzmann equation. Constructing numerical methods for this equation is a challenge, due in part to the kinetic theory description of moving particles, which relies on space, time, and velocity variables. Two novel approaches are presented and compared. The first uses a spectral collocation basis in velocity space. The resulting system is solved in time using Diagonally Implicit Runge-Kutta methods, chosen in order to mitigate stiffness concerns. A Jacobian-Free Newton—Krylov method is presented, accelerated with a sweeping preconditioner. The method is tested on 1D and 2D problems in order to validate its convergence behavior and investigate its efficiency. The second method uses DG for moment equations, which can be derived as spectral methods in velocity space with spatial and temporal adaptivity. These methods were first proposed in 1949 by Grad, but their applicability has been limited. The equations are not guaranteed to be hyperbolic, leading to stability issues. The elegance and potential for cost-reduction of Grad's moment method have led to the development of different moment closures that preserve hyperbolicity and model accuracy. The approaches studied in this thesis, the globally hyperbolic moment methods, restore hyperbolicity by introducing a term that cannot be written in conservative form. The equations are typically solved with operator splitting and low-order methods. We examine the promise and challenges of applying a high-order DG method with explicit Runge-Kutta time-stepping to these equations on common 1D test cases. The thesis ends with a discussion on the prospects of both methods and suggestions for future work.

Thesis Supervisor: Jaime Peraire
Title: H.N. Slater Professor of Aeronautics and Astronautics

Thesis Supervisor: Ngoc-Cuong Nguyen
Title: Principal Research Scientist

Acknowledgments

First and foremost I must thank my advisors Professor Jaime Peraire and Dr. Ngoc-Cuong Nguyen, who have helped me grow as a researcher and person. Their patience and insight have been invaluable to me and I am truly grateful for the opportunity to work alongside them.

I would also like to thank the administrative staff for going above and beyond to help make my experience at MIT as smooth as possible, in even the most chaotic of times. This includes Kate Nelson, Jean Sofronas, Beth Marois, and any others who I have not had the privilege of meeting.

Thank you to my friends at MIT and around the country who have kept me in good spirits.

Lastly I want to thank my parents and brother for the unwavering support.

Contents

List of Figures

List of Tables

Chapter 1

Introduction

Flow in extreme conditions, like the high speeds experienced by vehicles entering the atmosphere or the small scales of microelectromechanical systems, may not be well described as a continuum. In such regimes, collisions between particles become increasingly rare and thermodynamic equilibrium can no longer be assumed. Instead, the Boltzmann equation, derived from kinetic theory, may be required. The equation describes the movement of particles streaming and colliding at a statistical level, rather than tracking each particle individually.

In these regimes, particularly for hypersonic flows, setting up experiments can be a challenge [47]. Therefore, predictive numerical simulation plays an important role in studying these effects.

Probabilistic methods like Direct Simulation Monte Carlo (DSMC) [6] have proven effective for numerically solving the Boltzmann equation. There are, however, regimes of interest where DSMC loses efficiency; this motivates the development of deterministic methods for the Boltzmann equation.

Increasing computational power has made typically costly deterministic methods more feasible in the last few decades [22]. One reason for the cost of these methods is dimensionality; the solution of the Boltzmann equation depends not only on space and time, but also on velocity.

The treatment of this velocity domain, or velocity space, is a key differentiatior between deterministic methods. A common method is to directly discretize a trun-

cated velocity space. These methods allow for an arbitrarily rich discretization of the velocity space, meaning they can describe a very wide range of physical phenomena. In practice though, great care must be taken to avoid a proliferation of degrees of freedom [22, 24].

Another approach is to attempt to derive model equations that take into account velocity space information. Here we consider the moment equations, which track the evolution of moments of a velocity distribution function (vdf). Moment equations are usually valid only in certain physical regimes, but when applicable they present an opportunity to dramatically reduce computational cost. Significant effort has gone into deriving moment methods that are more descriptive and robust, particularly in regimes where probabilistic methods and direct discretizations become very costly [79].

Both approaches give systems of PDEs in space and time, which can then be solved using classic methods for numerical PDEs. Finite volume (FV) methods are often used [22, 58, 70], while semi-Lagrangean methods have had impressive results for direct discretizations of the Boltzmann equation [24, 23, 25] and finite element methods have recently been investigated for moment equations [82, 78].

In this thesis, we investigate the discontinuous Galerkin (DG) method for the Boltzmann equation, in particular for a certain class of globally hyperbolic moment methods [30]. DG possesses a number of attractive properties including easy extensions to high-order, stable discretizations for a wide range of operators, discretely-enforced conservativity, and the potential for local adaptivity. This comes at the price of increased computational cost. Despite the fact that computational cost is already seen as a barrier for the Boltzmann equation, there has been recent interest in using DG for direct discretizations [44, 76, 75, 28]. DG is less commonly used for the moment equations [7, 1].

The next chapter explains in greater detail the theory behind the Boltzmann equation and deterministic methods that aim to solve it. We focus on the theoretical results that are most relevant to the moment methods, including equilibrium states and asymptotics.

Chapter 3 focuses on the details of our DG methods. These include a novel implicit DG method for a direct solution of the Boltzmann equation and an explicit method for the moment equations. The shortcomings of the former inspired the investigation of the latter.

Numerical results are shown in Chapter 4. Reflections on these results and directions for future research are given in Chapter 5.

Chapter 2

Background

2.1 The Boltzmann Equation

The Boltzmann equation describes the evolution of a nonnegative velocity distribution function (vdf) $f(t, x, \xi)$, which evaluates to the number density of particles with velocity $\xi \in \mathbb{R}^{d_\xi}$ at position $x \in \mathbb{R}^{d_x}$ and time $t \in \mathbb{R}^+$. Here we will assume $d_x = d_\xi = d$. The equation can be written as

$$\frac{\partial f}{\partial t} + \xi \cdot \nabla_x f = \frac{1}{\tau} C(f, f) \tag{2.1}$$

and is defined on a spatial domain $\Omega \subseteq \mathbb{R}^d$, temporal domain $t \in [0, t_f]$, and velocity domain $\Xi = \mathbb{R}^d$. The right-hand side involves the relaxation time τ and the collision operator C. The relaxation time can depend on different parameters but will always vary based on the Knudsen number Kn. The Knudsen number is defined as the ratio

$$\mathrm{Kn} = \frac{\lambda}{L}. \tag{2.2}$$

L is a characteristic length scale, which is problem dependent. In the numerator is λ, or the mean-free path, which describes how far a particle will go before a collision occurs. A small Kn means that particles are frequently colliding without much free motion, allowing continuum descriptions of a group of particles to suffice. As Kn

grows larger, particles are in free motion for longer, leading to rarefied gases. This description can be made more mathematically precise, but the physical intuition is helpful: as Kn increases, a continuum gas becomes more rarefied, transitioning into kinetic regimes and eventually into free flight, where particles are travelling unimpeded.

2.1.1 Collisions and Macroscopic Moments

Collision operators are constructed to preserve mass, momentum, and energy. Respectively, this means that

$$\int_{\mathbb{R}^d} C(f,f)\psi(\xi)d\xi = 0 \tag{2.3}$$

for $\psi(\xi) = (1, \xi, |\xi|^2)$. The component functions of ψ are sometimes called the *elementary collision invariants* because they span the space of collision invariants [18].

The same operation in (2.3) can be applied to both sides of the Boltzmann equation (2.1). This gives a system of balance laws

$$\frac{\partial}{\partial t}\int_{\mathbb{R}^d} \psi_i f d\xi + \nabla \cdot \int_{\mathbb{R}^d} \xi\psi_i f d\xi = 0 \tag{2.4}$$

which is not a closed system since it involves higher-order moments of f.

The inner products of f and the collision invariants are weighted averages of a distribution which describe macroscopic quantities of interest. Specifically, we have relationships for the density ρ, the macroscopic momentum ρv, and the energy ρE

$$\rho = \int_{\mathbb{R}^d} f(t,x,\xi)d\xi \tag{2.5}$$

$$\rho v = \int_{\mathbb{R}^d} \xi f(t,x,\xi)d\xi \tag{2.6}$$

$$\rho E = \frac{1}{2}\int_{\mathbb{R}^d} |\xi|^2 f(t,x,\xi)d\xi. \tag{2.7}$$

where ρE is related to the temperature θ by

$$\rho E = \frac{1}{2}\rho|v|^2 + \frac{d}{2}\rho\theta.$$

H-Theorem and Equilibrium

Collision operators for the Boltzmann equation satisfy the *Boltzmann inequality*:

$$\mathcal{S} = \int_{\mathbb{R}^d} C(f,f)\log(f)d\xi \leq 0. \tag{2.8}$$

If $\mathcal{S} = 0$ then $\log(f)$ is a collision invariant. Therefore, $\log(f) = a + b\cdot\xi + c|\xi|^2$ or f is an exponential function. We can determine the values of a, b, and c by enforcing that f and the exponential have the same density, velocity, and temperature. This function is referred to as the *local Maxwellian*

$$\mathcal{M}(f)(t,x) = \frac{\rho(t,x)}{\sqrt{2\pi\theta(t,x)}}\exp\left(-\frac{|\xi - v(t,x)|^2}{2\theta(t,x)}\right) \tag{2.9a}$$

$$\rho(t,x) = \int_{\mathbb{R}^d} f(t,x,\xi)d\xi; \quad v = \frac{1}{\rho(t,x)}\int_{\mathbb{R}^d}\xi f(t,x,\xi)d\xi; \tag{2.9b}$$

$$\theta(t,x) = \frac{1}{\rho(t,x)}\int_{\mathbb{R}^d}(\xi - v(t,x))^2 f(t,x,\xi)d\xi. \tag{2.9c}$$

In the space homogeneous case, we can multiply both sides of (2.1) by $\log(f)$ to get

$$\frac{\partial}{\partial t}\int_{\mathbb{R}^d} f\log(f)d\xi = S \leq 0. \tag{2.10}$$

This is an entropy inequality where the entropy $\mathcal{H} = \int f\log(f)d\xi$ is always decreasing. At equilibrium, entropy has stopped changing, or $\mathcal{S} = 0$. This happens when f is equal to its local Maxwellian, which is why this distribution is sometimes referred to as the local equilibrium distribution. The proof of this for the space-inhomogenous case can be found in [18] and leads to a similar conclusion. Both cases imply irreversibility of the Boltzmann dynamics due to a decreasing entropy function.

As $\tau \to 0$, $C(f,f) \to 0$ and f becomes $\mathcal{M}(f)$. In this case, (2.4) becomes the

compressible Euler equations

$$\partial_t \begin{pmatrix} \rho \\ \rho v \\ \rho E \end{pmatrix} + \nabla_x \cdot \begin{pmatrix} \rho v \\ \rho v \otimes v + p\mathbb{I} \\ (\rho E + p)v \end{pmatrix} = 0 \tag{2.11}$$

with pressure $p = \rho\theta$.

In regimes of slight non-equilibrium, Chapman-Enskog theory can be used to obtain the Navier-Stokes equations from the Boltzmann equation as well [18].

2.1.2 Collision Operators

The right-hand side of (2.1) describes collisions between particles. The kinetic theory derivation of the Boltzmann equation leads to the operator

$$C(f, f) = \int_{\mathbb{R}^3} \int_{\mathbb{S}^2} (f' f'_* - f f_*) B(\xi, \xi_*, \theta) d\theta d\xi_* \tag{2.12}$$

where f' is the distribution post-collision and B is a collision kernel that varies based on the collision model. For each velocity, an integral needs to be taken over all other velocities and the unit hemisphere $\mathbb{S}^2$. This operator will be referred to as the *full* collision operator.While not implemented in this thesis, this operator plays an important role in influencing certain design choices of numerical methods for the Boltzmann equation.

Instead, we consider model collision operators, specifically the Bhatnagar-Gross-Krook (BGK) collision operator [5]. It describes relaxation towards equilibrium, defined as:

$$C(f, f) = \mathcal{M}(f) - f. \tag{2.13}$$

The BGK operator is clearly a significant simplification of the full operator. Despite this, it can still be useful in numerical simulations. First, the theory in the previous section mostly still applies; it obeys the same H-theorem and retains the asymptotic continuum behavior, albeit with an incorrect Prandtl number in the

Navier-Stokes limit. Note that the Prandtl number can be corrected with similar models like ellipsoidal statistical BGK and Shakhov operators. Furthermore, the BGK operator can be used to accelerate methods that use the full collision operator through operator penalization [26] or multi-fidelity models [17]. As a practical concern, the efficiency of the BGK model allows for the easier implementation of more complicated physical systems like reacting gases [70].

2.2 Deterministic Methods for the Boltzmann Equation

This section gives a brief overview of different numerical methods for the Boltzmann equation. While not comprehensive, we hope to emphasize some of the key factors that are considered when designing such methods. Particular emphasis is placed on different ways of treating velocity space.

2.2.1 Challenges

Despite focused efforts, solving the Boltzmann equation deterministically is a challenge. The first issue is dimensionality. Especially in 3D simulations, the velocity space increases compute times and can require prohibitive levels of memory.

Another issue is the computational treatment of the aforementioned asymptotics. In many flows of interest like rarefied hypersonic flow, the Knudsen number can vary drastically across the domain. As Kn goes to 0, the collision operator becomes stiff, necessitating smaller timesteps or implicit-in-time methods. On the other hand, as Kn increases, the flow can experience greater levels of nonequilibrium and require a richer disretization of velocity space in order to capture non-Maxwellian distributions. This is an inherently multiscale problem, necessitating the development of specialized schemes. These include methods that couple kinetic and continuum schemes targeting different Kn regimes [73, 34] and time-stepping schemes that discretely preserve asymptotics [46].

Perhaps the most daunting challenge in solving the Boltzmann equation is the collision operator. With N being the number of points in each velocity direction, direct implementations take N^6 operations. The fastest Fast Fourier Transform (FFT)-based methods for general collision kernels takes $O(MN^4 \log(N))$, where $M << N^2$ is the number of points on the unit sphere [36]. For the commonly used variable hard sphere (VHS) model, this can be reduced to $O(MN^3 \log(N))$ [32]. It is typical for the collision operator to dominate time-dependent problems [25, 51]. Note that the collision operator is local in physical space and is integrated over velocity space; this means that the velocity space representation is key in how the collision operator is evaluated.

2.2.2 Velocity Space Treatment

The most substantial difference between methods is how the velocity space is dealt with. Once that choice is made, what remains is a system of equations in space and time, which can be solved with more standard differential equation solvers.

Discrete Velocity Models

A common approach is to split the velocity space into evenly-spaced points and to solve a system of N equations that are coupled by the collision operator.

The first advantage of this is simplicity. Integration in velocity space can be calculated using equal spaced Newton-Cotes rules with no need to interpolate to quadrature nodes. In fact, it was recently pointed out in [19] that this method can be surprisingly effective for certain problems due to the spectral convergence of Newton-Cotes quadrature for smooth functions on infinite domains [80]. Furthermore, equal spaced grids abet the use of fast spectral methods.

A downside of this approach is that it requires truncating the velocity domain. This can make certain methods lose conservation of the moments, which can be dealt with through optimization methods first proposed in [64]. Bounds for the velocity domain must also be specified a priori or calculated using heuristics that approximate

the support of f [4]. This can be wasteful especially if the support of the f changes significantly over space or time.

2.2.3 Galerkin Methods in Velocity Space

Another approach is to expand f in terms of basis functions and enforce the equation in velocity space in a weak sense. We next review basis functions that are particularly effective in this context.

Orthogonal Polynomials

A set of polynomials $\{\phi_i\}_{i=1}^N$ that are orthogonal with respect to some weight function w and domain Ω (or equivalently, a choice of measure) are called orthogonal polynomials.

An advantage is that with particular choices of $w(x)$, Ω can be an infinite domain, making them a suitable basis for capturing pdfs without truncating velocity space. A relevant example are the probabilist's Hermite polynomials, which are defined as

$$He_n(x) = (-1)^n \exp\left(\frac{x^2}{2}\right) \frac{d^n}{dx^n}\left(\exp\left(-\frac{x^2}{2}\right)\right). \tag{2.14}$$

He_i are orthogonal on $\Omega = \mathbb{R}^n$ and $w(\xi) = \exp(-\xi^2/2)$. Specifically, the Hermite polynomials satisfy

$$\int_{\mathbb{R}} He_n(\xi) He_m(\xi) e^{\left(-\frac{\xi^2}{2}\right)} d\xi = n!\sqrt{2\pi}\delta_{nm} \tag{2.15}$$

where δ_{nm} is the Kronecker delta. They are a natural choice for the Boltzmann equation because the weight function is of the same form as the Maxwellian distribution.

All orthogonal polynomials satisfy a three term recurrence relation. The Hermite polynomials satisfy

$$He_{n+1}(x) = xHe_n(x) - nHe_n(x). \tag{2.16}$$

Hermite polynomials have been used extensively for Galerkin methods in velocity space [48, 43] and are also used to derive the moment equations described in the

following section and chapters.

Other orthogonal polynomials used for velocity space bases include Burnett Polynomials [42, 50] Polar-Laguerre polynomials [69], Half-space Hermite Polynomials [38], and Chebyshev Polynomials [41]. Some choices of velocity space basis functions do not always admit fast algorithms for the collision operator. They do possess a number of attractive qualities though, like more efficient representations of f and enforced conservation of the macroscopic quantities [37].

2.2.4 Adaptivity in Velocity Space

Before moving on to the macroscopic model equations, it is worth mentioning the concept of velocity space adaptivity, as it is both an approach for accelerating the aforementioned methods and a way to derive the moment equations to be described below.

Typically for the methods presented so far, every point in space shares the same velocity domain. This simplifies implementation greatly. However, it can be hugely wasteful. In the case of a gas in equilibrium with a velocity that varies in space, each distribution can be recovered with just five degrees of freedom at each point in space, but the velocity space discretization must be able to capture all distributions.

It has been pointed out that for hypersonic rarefied flow in particular, adaptive grids could be a requirement [3, 8]. The temperature and velocity can vary greatly across the domain, necessitating a velocity grid that extends far out and requires very fine spacing.

For discrete velocity methods, there have been recent attempts to use local velocity grids at different points in space [3, 4]. In a Galerkin method, it is the basis functions that vary in space. The most common approach is not to change the functions themselves at each point, but to shift and scale the velocity domain. This idea is practical because v and θ, due to their definition as the mean and variance of f, contain details of the support of f. If the velocity domain is shifted by the mean ($\tilde{\xi} = \xi - v$) and scaled by the variance ($\hat{\xi} = \tilde{\xi}/\sqrt{\theta}$), then $f(t, x, \hat{\xi})$ will be normalized in a sense. Distributions that could vary in width and location are now brought to

the origin and scaled to have similar widths.

In fact, it is common for Galerkin methods in velocity space to shift and scale their inputs by a constant characteristic velocity and temperature [49, 41]. Allowing the rescaling parameters to change in space and time complicates the PDE and introduces the question of how exactly should the parameters be determined. For example, [51] uses a predictor-corrector method while [33] uses the asymptotic equations.

2.3 Moment Equations

Another way to address the computational burden of the velocity space discretization is to avoid it entirely. As mentioned in Section 2.1.1, the Navier-Stokes equations can be derived from the Boltzmann equation using Chapman-Enskog theory. A higher-order extension of the same theory results in the Burnett and Super-Burnett equations. Unfortunately, these equations are in general not stable [79].

A more reliable approach stems from noticing that the continuum equations evolve integrated quantities, the moments, of f. In 1949, Grad derived the first *moment equations* for nonequilibrium gas dynamics [39]. While influential, fundamental issues with Grad's equations limited their applicability for realistic problems for a long time. This section explains Grad's equations and their limitations. We then describe methods that circumvent these limitations.

2.3.1 Grad's Method

Grad's method can be derived by expanding f as

$$f(t,x,\xi) = \sum_{\alpha=0}^{\infty} f_\alpha(t,x)\mathcal{H}_\alpha^{v,\theta}(\xi) \tag{2.17}$$

where the basis functions are shifted and scaled Hermite polynomials:

$$\mathcal{H}_\alpha^{v,\theta}(\xi) = \theta(t,x)^{-\alpha/2} He_\alpha\left(\frac{\xi - v(t,x)}{\sqrt{\theta(t,x)}}\right)\frac{1}{\sqrt{2\pi\theta(t,x)}}\exp\left(-\frac{|\xi - v(t,x)|^2}{2\theta(t,x)}\right).$$

Through this lens, Grad's method can be seen as an adaptive spectral method in velocity space, where the rescaling parameters are exactly the macroscopic moments, rather than approximations.

This expansion is plugged into (2.1), which results in an unclosed system of equations. Orthogonality of the Hermite polynomials means that $f_0 = \rho$ and the additional use of exact v and θ constrains $f_1 = f_2 = 0$. Grad's closure is to set $f_\alpha = 0$ for $\alpha \geq N$ for a fixed N. Coefficients f_α are then matched to form a system of equations. Following the notation of [9], Grad's system can be written compactly by defining a convective derivative $\frac{\mathrm{d}}{\mathrm{d}t} = \partial_t + v\partial x$ and a term

$$\mathcal{F}_\alpha = \partial_x f_\alpha + f_{\alpha-1}\partial_x v + \frac{1}{2} f_{\alpha-2}\partial_x \theta. \tag{2.18}$$

Then the system can be written as

$$\begin{aligned} \frac{\mathrm{d}f_\alpha}{dt} + \frac{\mathrm{d}v}{\mathrm{d}t} f_{\alpha-1} + \frac{1}{2}\frac{\mathrm{d}\theta}{\mathrm{d}t} f_{\alpha-2} + \theta\mathcal{F}_{\alpha-1} + (\alpha+1)\mathcal{F}_{\alpha+1} \\ = -\frac{1-\delta_{\alpha 0}}{\tau} f_\alpha \ ; \ \forall \alpha = 0, \ldots N-1 \end{aligned} \tag{2.19}$$

where any f_α with $\alpha \leq 0$ or $\alpha \geq N$ is set to 0.

2.3.2 Hyperbolicity

To understand the limited success of this system, we must define the concept of hyperbolicity. Suppose a system of PDEs has the form

$$\frac{\partial \boldsymbol{u}}{\partial t} + A(\boldsymbol{u})\frac{\partial \boldsymbol{u}}{\partial x} = S(\boldsymbol{u}). \tag{2.20}$$

If the system can be written in conservative form for some flux function F,

$$\frac{\partial \boldsymbol{u}}{\partial t} + \frac{\partial F(\boldsymbol{u})}{\partial x} = S(\boldsymbol{u}) \tag{2.21}$$

then $A(\boldsymbol{u})$ is the Jacobian of $F(\boldsymbol{u})$.

This system is hyperbolic if the eigenvalues of $A(\boldsymbol{u})$ are real and $A(\boldsymbol{u})$ is diagonal-

izable. The eigenvalues of A are the characteristic speeds of propagation. Imaginary characteristic speeds can result in unphysical behavior. Note that this definition does not involve the source term.

The hyperbolicity issue is particularly potent for Grad's equations. For 1 spatial dimension, the characteristic polynomial for Grad's system was shown to be

$$|\lambda I - A| = \theta^{\frac{N}{2}} He_N\left(\frac{\lambda - v}{\sqrt{\theta}}\right) - \frac{N!}{2\rho}\left((\lambda - v)^2 - \theta) f_{N-2} + 2(\lambda - v) f_{N-1}\right)$$

the roots of which are not guaranteed to be real. In 1D it has long been known Grad's method can fail for certain problems. In 3D however, there is no neighborhood around the local equilibrium for which $A(\boldsymbol{u})$ is hyperbolic everywhere in that neighborhood (specifically, an equilibrium Maxwellian $\boldsymbol{u}$ lies on the boundary of the hyperbolicity region rather than on the interior). This means in 3D that arbitrary perturbations can make the system lose hyperbolicity [13].

2.3.3 Modern moment methods

While Grad's method proved to be of limited practical use, significant work has gone into finding similar equations that are more reliable for a wider range of problems.

Some models change the way in which f is expanded. Examples include the quadrature-based moment methods, which expands f as a linear combination of delta functions [35], and the maximum entropy methods which enforce that f minimizes an entropy functional at every point [61, 1].

Another approach is to use the same or similar bases as Grad and to add terms to the equations that stabilize or regularize it. The regularized moment equations for example add a stabilizing diffusive source term [74]. An advantage of these models is that the added terms are directly related to physical quantities through constitutive relations [79]. Therefore, the study of these equations can reveal insight into the physics of a rarefied flow that might be otherwise obscured. The derivation of these models is not straightforward, however, making them a challenge to apply to different equations.

2.3.4 Framework for Globally Hyperbolic Moment Methods

We focus on the globally hyperbolic equations first derived in [10] for 1D and [12] for 3D. The Hyperbolic Moment Equations (HME) emphasize efficiency over the interpretability of the regularized methods, but they can be derived through rigorous frameworks that are easily extendable.

These methods use the same basis for f as a Grad's method but are constructed to be hyperbolic. They were first derived as correction to Grad's equations, with an added term that forces the characteristic speeds to be real [10].

Hyperbolic Moment Equations

Later, these equations were rederived as approximations to the Boltzmann equation, with an explicit procedure that we restate here. This approach was elucidated by the development of alternate hyperbolic moment equations such as [59]. The procedure, adopted from [11], is summarized as follows

1. Expand f in the adaptive Hermite basis: $f(t,x,\xi) = \sum_{\alpha=0}^{\infty} f_\alpha(t,x)\mathcal{H}_\alpha^{v,\theta}(\xi)$
2. Evaluate $\frac{\partial f}{\partial t}$, $\frac{\partial f}{\partial x}$, and $C(f,f)$ and expand the results in the same basis (though in general different choices of bases can be taken at each step).
3. Truncate the expansion of the terms from step 2 to a fixed N.
4. Evaluate the expression $\xi\frac{\partial f}{\partial x}$ and truncate the resulting series.
5. Insert the expressions for $\frac{\partial f}{\partial t}, \xi\frac{\partial f}{\partial x}$, and $C(f,f)$ into the Boltzmann equation and match coefficients for each basis function.

The truncation in step 3 is emphasized because it turns out to actually be the step that differs from Grad's method and the step that ensures hyperbolicity. Every operation, whether a derivative, multiplication, or the source term, must be treated in the same way: expanded in a chosen basis and truncated. The issues in Grad's method comes from not truncating the expansion of $\frac{\partial f}{\partial x}$ before multiplying it by the velocity. The

system of equations ends up being the same as (2.19) with the $\mathcal{F}_{\alpha+1}$ term in the last equation removed:

$$\frac{\mathrm{d}f_\alpha}{\mathrm{d}t} + \frac{\mathrm{d}v}{\mathrm{d}t} f_{\alpha-1} + \frac{1}{2}\frac{\mathrm{d}\theta}{\mathrm{d}t} f_{\alpha-2} + \theta\mathcal{F}_{\alpha-1} + (1-\delta_{N-1,\alpha})(\alpha+1)\mathcal{F}_{\alpha+1} = -\frac{1-\delta_{\alpha 0}}{\tau} f_\alpha \ ; \ \forall \alpha = 0, \dots N-1. \tag{2.22}$$

For numerical methods an equivalent conservative form is typically preferred; as such it will be used in chapter 3. Still, this formulation is useful for analysis. Note that using this form, it was recently proved in [63] that HME retains the correct asymptotic Navier-Stokes limit.

It can be shown that the characteristic speeds for this system are the roots of $He_N\left(\frac{\lambda - v}{\sqrt{\theta}}\right)$, confirming that the roots are real and the system is hyperbolic.

Highest-Moment-Based Hyperbolic Moment Method

While this correction has increased the usability and versatility of hyperbolic moment methods, there is a limit to their applicability.

The derivation repeatedly assumes that the infinite sum $\sum_\alpha f_\alpha \mathcal{H}_\alpha$ converges. As pointed out in [16], this is not always a valid assumption. The series can diverge when trying to represent the sum of two Maxwellians with a large enough difference in temperature. A new moment method was recently proposed in [9] that avoids this issue while keeping most of the structure of HME. It is termed the Highest-Moment-Based Moment Method (HMBMM) due to a rescaling that instead of using θ, uses the $N-1$-th centered moment, Θ

$$\Theta(t,x) = \left(\frac{1}{(N-2)!!\rho(t,x)} \int_{\mathbb{R}} (\xi - v(t,x))^{N-1} f(t,x,\xi) d\xi \right)^{2/(N-1)}. \tag{2.23}$$

The expressions are different for even and odd N, since the $N-1$-th centered moment of the equilibrium distribution is zero if N is even. For simplicity we assume for HMBMM that N is always odd.

Now f is expanded with basis functions $\mathcal{H}^{v,\Theta}$. The choice of Θ guarantees that

this expansion can converge to any linear combination of Maxwellian distributions.

The steps for deriving a hyperbolic system of equations can be repeated with this basis, with many of the expressions being similar. For example, the characteristic speeds are now the roots of $He_N\left(\frac{\lambda-v}{\sqrt{\Theta}}\right)$. The system of equations is

$$\frac{\mathrm{d}f_\alpha}{\mathrm{d}t} + \frac{\mathrm{d}v}{\mathrm{d}t} + \frac{1}{2}\frac{\mathrm{d}\Theta}{\mathrm{d}t} f_{\alpha-2} + \Theta\mathcal{F}_{\alpha-1} + (1-\delta_{N-1,\alpha}(\alpha+1)\mathcal{F}_{\alpha+1} \tag{2.24a}$$

$$= \frac{1}{\tau}\left[\frac{1+(-1)^\alpha}{2}\frac{f_0}{\alpha!!}\left(\frac{2f_2}{f_0}\right)^{\alpha/2} - f_\alpha\right],\ \forall\alpha = 0, 1, \ldots N-1. \tag{2.24b}$$

Note that while f_1 is still constrained to equal 0, the use of Θ introduces a new constraint on f_{N-1} rather than f_2:

$$f_{N-1} = \sum_{\alpha=2;\ \alpha\ \text{even}}^{N-3} \frac{f_\alpha \Theta^{(N-1-\alpha)/2}}{(N-1-\alpha)!!}. \tag{2.25}$$

While the unknowns for HME are $f_0, v, \theta, f_3, \ldots f_{N-1}$, the unknowns for HMBMM are $f_0, v, f_2, \ldots, f_{N-2}, \Theta$.

It is not yet known whether this method preserves the Navier-Stokes asymptotics in general, though [9] proved the Euler limit for $N = 5$.

Projection-based Framework

Before describing our numerical implementation of these equations, we note that they can also be described in a more general projection-based framework [11, 30]. For example, the truncations above can be explained as the projection into a finite dimensional function space spanned by the adaptive Hermite polynomials [30].

While not necessary here as we use previously-derived methods, this enables the systematic derivation of different hyperbolic models, both for the Boltzmann equation with different bases [31, 57] and different equations entirely [60, 21, 55, 27].

Chapter 3

Formulation of DG Methods for the Boltzmann Equation

This chapter details the DG methods investigated in this thesis. The first method directly solves for the velocity distribution function f, using spectral collocation in velocity space with implicit time stepping by means of a Jacobian-Free Newton–Krylov (JFNK) method. The second method evolves the moments of the distribution using the framework described in Section 2.3.4 through the use of a DG discretization and explicit time integration.

3.1 Preliminaries

3.1.1 Notation

Let $\Omega \in \mathbb{R}^d$ be a domain with Lipschitz boundary $\partial\Omega \in \mathbb{R}^{d-1}$. A disjoint partition of the domain is a triangulation $\mathcal{T}_h$. Elements that partition the domain are denoted $K \in \mathcal{T}_h$ and the boundary of each element is ∂K.

We also define $\mathcal{P}^k(D)$ to be the polynomials of at most order k on the domain D and $L^2(D)$ as the space of square-integrable functions on D.

Common to all DG methods is the need to define a numerical flux. For an analytic flux F, the corresponding numerical flux will be denoted $\widehat{F}$. The numerical flux

depends on the solution on a face $E \in \partial K \cup \partial\Omega$. Due the discontinuous nature of the approximation spaces, the solution on E is double valued. Then, for $y(\boldsymbol{x})$ on face E of element K, we define $y^+(\boldsymbol{x})$ to be the value on the interior of the element and $y^-(\boldsymbol{x})$ to be the corresponding value in the neighbor element.

3.1.2 Approximation Spaces

We define the discontinuous approximation spaces

$$\mathcal{W}_h^k = \{w \in L^2(\mathcal{T}_h) \ : \ w|_k \in \mathcal{P}^k(K) \ , \ \forall K \in \mathcal{T}_h\} \tag{3.1}$$

$$\mathcal{V}_h^k = \{\boldsymbol{v} \in L^2(\mathcal{T}_h) \ : \ \boldsymbol{v}|_k \in (\mathcal{P}^k(K))^d, \ \forall K \in \mathcal{T}_h\}. \tag{3.2}$$

We also require inner products on the triangulation and its boundaries:

$$(\boldsymbol{a}, \boldsymbol{b})_{\mathcal{T}_h} = \sum_{K \in \mathcal{T}_h} \int_K \boldsymbol{a} \cdot \boldsymbol{b} \tag{3.3}$$

$$\langle \boldsymbol{a}, \boldsymbol{b} \rangle_{\partial\mathcal{T}_h} = \sum_{\partial K \in \partial\mathcal{T}_h} \int_{\partial K} \boldsymbol{a} \cdot \boldsymbol{b} \tag{3.4}$$

These approximation spaces and inner products will be used to derive semi-discrete systems that depend on a continuous time derivative.

3.1.3 Time Integration

The two methods presented below use different strategies for time integration, but both are advanced in time using the Runge-Kutta (RK) schemes [81]. The semi-discrete systems can be cast in the form

$$\frac{dy}{dt} = g(t, y).$$

for an evolved quantity y and function g. The time domain is split into discrete times $t_0 = t^1, t^2, \ldots, t^{L-1}, t^L = t_f$ and the approximation of y at timestep ℓ is y^ℓ. To

advance from y^ℓ to $y^{\ell+1}$ with $t^{\ell+1} - t^\ell = \Delta t$, an s-stage RK method uses

$$y^{\ell+1} = y^\ell + \sum_{i=1}^{s} b_i g(t^{\ell,i}, y^{\ell,i}) \tag{3.5a}$$

$$y^{\ell,i} = g\left(t + c_i \Delta t, y^\ell + \Delta t \sum_{j=1}^{s} a_{i,j} y^{\ell,j}\right), \quad i,j = 1, \dots s. \tag{3.5b}$$

RK methods can be expressed compactly with Butcher tableaus

$$\begin{array}{cccc|c} a_{11} & a_{12} & \dots & a_{1s} & c_1 \\ a_{21} & a_{22} & \dots & a_{2s} & c_2 \\ \vdots & \vdots & \dots & \vdots & \vdots \\ a_{s1} & a_{s2} & \dots & a_{ss} & c_s \\ \hline b_1 & b_2 & \dots & b_s & \end{array} . \tag{3.6}$$

If $a_{ij} = 0$ for $i < j$ then the method is a Diagonally implicit Runge-Kutta (DIRK) scheme. If $a_{ij} = 0$ for $i \leq j$, the method is an Explicit Runge-Kutta (ERK) method.

Explicit methods are usually less computationally expensive, but the time step size is limited in the presence of small grid size or numerical stiffness. This restriction is avoided in implict methods at the cost of requiring a nonlinear solve at each stage [81]. This is particularly relevant for the Boltzmann equation, because as mentioned in Section 2.2.1 the equation becomes stiff as $\tau \to 0$ [46].

3.2 Implicit DG for the Boltzmann-BGK Equation

This method approximates the velocity distribution function f with a spectral collocation method in velocity space. The velocity space is expanded with basis functions, much like the Galerkin methods of Section 2.2.3. The particular choice of basis is such that the Boltzmann equation needs to be solved only at discrete velocities called collocation points, similar to the discrete velocity methods described in Section 2.2.2. A collocation method was used in [38], but with different choices of collocation points, bases, and numerical methods.

3.2.1 Velocity Space Collocation

To approximate f, we use continuous basis functions in the velocity domain, $\{\phi_i(\boldsymbol{\xi})\}_{\alpha=1}^{N}$ where $\boldsymbol{\xi} \in \mathbb{R}^d$. Specifically, f evaluated at a velocity $\boldsymbol{\xi}^*$ is approximated as

$$f(t, \boldsymbol{x}, \boldsymbol{\xi}^*) \approx \sum_{\alpha=1}^{N} f_\alpha(t, \boldsymbol{x}) \phi_\alpha(\boldsymbol{\xi}^*) \tag{3.7}$$

We also assume a given set of N collocation points $\{\boldsymbol{\xi}_\alpha\}_{\alpha=1}^{N}$ such that $\phi_i(\boldsymbol{\xi}_\alpha) = \delta_{i\alpha}$. This means that the coefficients of the expansion (3.7) are given by $f_\alpha(t, \boldsymbol{x}) = f(t, \boldsymbol{x}, \boldsymbol{\xi}_\alpha)$. The collocation method enforces the Boltzmann equation (2.1) at the collocation points

$$\frac{\partial f_\alpha(t, \boldsymbol{x})}{\partial t} + \boldsymbol{\xi}_\alpha \cdot \nabla_{\boldsymbol{x}} f_\alpha(t, \boldsymbol{x}) - \frac{1}{\tau} \left(\mathcal{M}(\boldsymbol{f}) - f_\alpha(t, \boldsymbol{x}) \right) = 0, \quad \alpha = 1, \ldots, N \tag{3.8}$$

where $\boldsymbol{f} = (f_1, \ldots f_N)$. Note that this system is coupled through the collision term, particularly through the function $\mathcal{M}(\boldsymbol{f})$ from the BGK operator (2.13). Calculating the local Maxwellian of f, while local in space, requires evaluating integrals over all velocity space to calculate the macroscopic moments by equations (2.5) - (2.7). With the velocity space basis, the operations for the macroscopic moments can be evaluated as

$$\int_{\mathbb{R}^d} \psi(\boldsymbol{c}) f(t, \boldsymbol{x}, \boldsymbol{\xi}) = \sum_{\alpha=1}^{N} f_\alpha \int_{\mathbb{R}^d} \psi(\boldsymbol{\xi}) \phi_\alpha(\boldsymbol{\xi}) d\xi = \sum_{\alpha=1}^{N} f_\alpha \boldsymbol{a}_\alpha. \tag{3.9}$$

The integrals for the coefficients $\boldsymbol{a}_\alpha$ in (3.9) can be precomputed.

The velocity space basis can be any collection of spectral basis functions. Here we use a tensorized basis similar to those developed for spectral element methods [66]. Minimum and maximum velocities are specified a-priori and the interval between them is divided into elements. A piecewise polynomial basis is constructed with Lagrange polynomials inerpolating at Chebyshev nodes within each element. The higher dimensional basis is created by taking the tensor product of this 1D basis.

3.2.2 Weak Form

The spectral collocation results in N transport equations with a nonlinear source term. The weak form of this system is as follows: for all f_α, find an approximation $f_{\alpha,h} \in \mathcal{W}_h^k$ that satisfies

$$\left(\frac{\partial f_{\alpha,h}}{\partial t}, w\right)_{\mathcal{T}_h} - (\boldsymbol{\xi}_\alpha f_{\alpha,h}, \nabla_{\boldsymbol{x}} w)_{\mathcal{T}_h} + \left\langle (\boldsymbol{\xi}_\alpha \cdot \boldsymbol{n}) \widehat{f}_{\alpha,h}, w \right\rangle_{\partial \mathcal{T}_h} + \left(\frac{1}{\tau}\left(f_{\alpha,h} - \mathcal{M}(\boldsymbol{f}_h)\right), w\right)_{\mathcal{T}_h} = 0, \quad t \in (0, t_f],\ \forall w \in \mathcal{W}_h^k, \tag{3.10}$$

where $\boldsymbol{f}_h = (f_{1,h}, \dots f_{N,h})$ and

$$(\boldsymbol{\xi}_n \cdot \boldsymbol{n}) \widehat{f}_{\alpha,h}(t, \boldsymbol{x}) = \begin{cases} (\boldsymbol{\xi}_\alpha \cdot \boldsymbol{n}) f_{n,h}(t, \boldsymbol{x}), & \text{if } \boldsymbol{\xi}_\alpha \cdot \boldsymbol{n} \geq 0 \\ (\boldsymbol{\xi}_\alpha \cdot \boldsymbol{n}) f^-_{n,h}(t, \boldsymbol{x}), & \text{if } \boldsymbol{\xi}_\alpha \cdot \boldsymbol{n} < 0 \text{ and } E \notin \partial\Omega \\ (\boldsymbol{\xi}_\alpha \cdot \boldsymbol{n}) f_D(t, \boldsymbol{x}, \boldsymbol{c}_n), & \text{if } \boldsymbol{\xi}_\alpha \cdot \boldsymbol{n} < 0 \text{ and } E \in \partial\Omega \end{cases} \tag{3.11}$$

for far-field boundary conditions f_D.

3.2.3 Solution Method and Preconditioning

Equation (3.10) is solved with DIRK time integration. Let $\boldsymbol{f}_h^\ell$ be $\boldsymbol{f}_h$ at timestep ℓ. We assume that the same velocity space basis is used at every point in space, so that $\boldsymbol{f}_h^\ell \in \mathbb{R}^{NM}$ where M is the number of degrees in $\mathcal{T}_h$. Then we can associate a residual $\boldsymbol{r}_\alpha$ that takes the same form for each equation in (3.10):

$$\boldsymbol{r}_\alpha(\boldsymbol{f}_h^\ell) \equiv \boldsymbol{A}_\alpha f_{\alpha,h}^\ell + \boldsymbol{g}_\alpha(\boldsymbol{f}_h^\ell) + \boldsymbol{b}_\alpha^\ell. \tag{3.12}$$

The terms in the residual are associated with the inner products in (3.10): $\boldsymbol{A}_\alpha$ is associated with bilinear terms, $\boldsymbol{g}_\alpha$ with the nonlinear part of the collision term, and $\boldsymbol{b}_\alpha$ with the linear terms due to the time discretization and boundary terms.

We define a vector of residuals $\boldsymbol{r}(\boldsymbol{f}_h^\ell) = (\boldsymbol{r}_1(\boldsymbol{f}_h^\ell), r_2(\boldsymbol{f}_h^\ell), \dots, \boldsymbol{r}_N(\boldsymbol{f}_h^\ell)) \in \mathbb{R}^{NM}$. Similarly we define $\boldsymbol{g}(\boldsymbol{f}_h^\ell) := (\boldsymbol{g}_1(\boldsymbol{f}_h^\ell), \boldsymbol{g}_2(\boldsymbol{f}_h^\ell), \dots, \boldsymbol{g}_N(\boldsymbol{f}_h^\ell))$, $\boldsymbol{b}^\ell := (\boldsymbol{b}_1^\ell, \boldsymbol{b}_2^\ell, \dots, \boldsymbol{b}_N^\ell)$, and

block diagonal matrix $\boldsymbol{A} = \text{diag}(\boldsymbol{A}_1, \boldsymbol{A}_2, \ldots, \boldsymbol{A}_N)$. Each stage of the DIRK scheme will require finding the roots of the following nonlinear system of equations

$$\boldsymbol{r}(\boldsymbol{f}_h^\ell) \equiv \boldsymbol{A}\boldsymbol{f}_h^\ell + \boldsymbol{g}(\boldsymbol{f}_h^\ell) - \boldsymbol{b}^\ell = 0. \tag{3.13}$$

Equation (3.13) is solved with Newton's method. At iteration k of Newton's method, the Newton step $\delta\boldsymbol{f}_h^{\ell,k}$ is determined by solving

$$(\boldsymbol{A} + \boldsymbol{J}^{\ell,k})\ \delta\boldsymbol{f}_h^{\ell,k} = -\left(\boldsymbol{A}\boldsymbol{f}_h^{\ell,k} + \boldsymbol{g}(\boldsymbol{f}_h^{\ell,k}) - \boldsymbol{b}^\ell\right). \tag{3.14}$$

where $\boldsymbol{J}^{\ell,k}$ is the Jacobian of $\boldsymbol{g}(\boldsymbol{f}_h^{\ell,k})$. For the initial guess of each Newton iteration, we take the solution from the previous timestep, $\boldsymbol{f}_h^{\ell-1}$. The linear system (3.14), likely too large to be solved with a direct method, is solved with preconditioned GMRES.

Computing the preconditioner

As a preconditioner, we use the inverse of $\boldsymbol{A}$. Since $\boldsymbol{A}$ is block diagonal, its inverse is also block diagonal. The action of this preconditioner on a vector $\boldsymbol{z} = (\boldsymbol{z}_1, \ldots, \boldsymbol{z}_N)$ requires the evaluation of $\boldsymbol{A}^{-1}\boldsymbol{z}$. Equivalently, we must solve N linear systems of the form

$$\boldsymbol{A}_\alpha \boldsymbol{y}_\alpha = \boldsymbol{z}_\alpha, \quad \alpha = 1, \ldots, N. \tag{3.15}$$

Recall that each $\boldsymbol{A}_\alpha$ corresponds to the bilinear terms in (3.10). The matrix-vector multiplication in (3.15) is therefore equivalent to the following DG weak form

$$(\beta y_{\alpha,h}, w)_{\mathcal{T}_h} - (\boldsymbol{\xi}_\alpha y_{\alpha,h}, \nabla_{\boldsymbol{x}} w)_{\mathcal{T}_h} + \langle (\boldsymbol{\xi}_\alpha \cdot \boldsymbol{n})\widehat{y}_{\alpha,h}, w\rangle_{\partial\mathcal{T}_h} = (z_\alpha, w)_{\mathcal{T}_h}, \quad \forall w \in \mathcal{W}_h^k, \tag{3.16a}$$

where β is a constant arising from DIRK scheme and

$$(\boldsymbol{\xi}_\alpha \cdot \boldsymbol{n})\widehat{y}_{\alpha,h} = \begin{cases} (\boldsymbol{\xi}_\alpha \cdot \boldsymbol{n}) y_{\alpha,h}, & \text{if } \boldsymbol{\xi}_\alpha \cdot \boldsymbol{n} \geq 0 \\ (\boldsymbol{\xi}_\alpha \cdot \boldsymbol{n}) y^-_{\alpha,h}, & \text{if } \boldsymbol{\xi}_\alpha \cdot \boldsymbol{n} < 0 \text{ and } F \notin \partial\Omega_h \\ 0 & \text{if } \boldsymbol{\xi}_\alpha \cdot \boldsymbol{n} < 0 \text{ and } F \in \partial\Omega_h. \end{cases} \tag{3.16b}$$

Note that the boundary value is set to 0 since the boundary conditions in (3.12) are contained in $\boldsymbol{b}_\alpha^\ell$. Due to the equivalency between (3.15) and (3.16), an efficient solution of (3.16) will be an efficient application of the preconditioner.

To solve this, we make use of a sweeping technique, commonly used for neutron transport [65]. We focus on the weak form in a single element $K \in \mathcal{T}_h$. Let $\partial K^- = \{\boldsymbol{x} \in \partial K \ : \ \boldsymbol{\xi}_\alpha \cdot \boldsymbol{n} < 0\}$. Then we can use (3.16b) to more explicitly write out the boundary integral term in (3.16a) to get

$$\begin{aligned}(\beta y_{\alpha,h}, w)_K - (\boldsymbol{\xi}_\alpha y_{\alpha,h}, \nabla_{\boldsymbol{x}} w)_K + \langle (\boldsymbol{\xi}_\alpha \cdot \boldsymbol{n}) y_{\alpha,h}, w \rangle_{\partial K \setminus \partial K^-} \\ = (z_\alpha, w)_K - \left\langle (\boldsymbol{\xi}_\alpha \cdot \boldsymbol{n}) y^-_{\alpha,h}, w \right\rangle_{\partial K^-}, \quad \forall w \in \mathcal{W}_h^k,\end{aligned} \tag{3.17}$$

If the value of $y^-_{\alpha,h}$ is known, then we are able to solve for $y_{\alpha,h}$ on element K.

To solve for $y_{\alpha,h}$ on the whole domain, we first let S_0 be the set of elements where $\partial K^- \subset \partial\Omega$. For $K \in S_0$, (3.17) becomes

$$(\beta y_{\alpha,h}, w)_K - (\boldsymbol{\xi}_\alpha y_{\alpha,h}, \nabla_{\boldsymbol{x}} w)_K + \langle (\boldsymbol{\xi}_\alpha \cdot \boldsymbol{n}) y_{\alpha,h}, w \rangle_{\partial K \setminus \partial K^-} = (z_\alpha, w)_K, \quad \forall w \in \mathcal{W}_h^k, \tag{3.18}$$

so the solution on these elements can be computed without requiring information from neighboring elements. Let S_1 be the set of elements for which ∂K^- are also faces on elements in S_0. Once the solution in all of S_0 is known, the solution in S_1 can be calculated by (3.17). This process can be repeated throughout the domain, sequentially sweeping from one set of elements to the next and solving for $y_{\alpha,h}$ in every element K.

Therefore, $\boldsymbol{y}_\alpha$ can be solved in an element-by-element fashion, providing an element-by-element method for computing the action of a single block of the preconditioner. To apply the entire preconditioner, this process must be applied for all collocation points $\boldsymbol{\xi}_\alpha$, each corresponding to a different sweep through the domain. The preconditioner can be applied in parallel, and since the collocation points are fixed, the orderings of the elements and the inverse of each $\boldsymbol{A}_\alpha$ can be precomputed and stored.

Jacobian-Free Newton Krylov method

After applying $\boldsymbol{A}^{-1}$, (3.14) becomes

$$(\boldsymbol{I} + \boldsymbol{A}^{-1}\boldsymbol{J}^{\ell,s})\ \delta \boldsymbol{f}_h^{\ell,s} = -\left(\boldsymbol{f}_h^{\ell,s} + \boldsymbol{A}^{-1}\left(\boldsymbol{g}(\boldsymbol{f}_h^{\ell,s}) - \boldsymbol{b}^{\ell}\right)\right). \tag{3.19}$$

For GMRES, instead of storing $(\boldsymbol{I} + \boldsymbol{A}^{-1}\boldsymbol{J}^{\ell,s})$ we need to know its application to a vector:

$$(\boldsymbol{I} + \boldsymbol{A}^{-1}\boldsymbol{J}^{\ell,s})\boldsymbol{y} = \boldsymbol{y} + \boldsymbol{A}^{-1}\boldsymbol{J}^{\ell,s}\boldsymbol{y}. \tag{3.20}$$

The matrix $\boldsymbol{J}^{\ell,s}$ is the Jacobian of $\boldsymbol{g}(\boldsymbol{f}_h^{l,s})$, which can be approximated with a finite difference

$$\boldsymbol{J}^{\ell,s}\boldsymbol{y} = \frac{\partial \boldsymbol{g}(\boldsymbol{f}_h^{\ell,s})}{\partial \boldsymbol{f}_h}\,\boldsymbol{y} \approx \frac{\boldsymbol{g}(\boldsymbol{f}_h^{\ell,s} + \epsilon\boldsymbol{y}) - \boldsymbol{g}(\boldsymbol{f}_h^{\ell,s})}{\epsilon} \tag{3.21}$$

for small ϵ [53]. Accordingly, the matrix-vector application needed for GMRES is approximated as

$$(\boldsymbol{I} + \boldsymbol{A}^{-1}\boldsymbol{J}^{\ell,s})\ \delta \boldsymbol{f}_h^{\ell,s} \approx \boldsymbol{y} + \frac{1}{\epsilon}\boldsymbol{A}^{-1}\left(\boldsymbol{g}(\boldsymbol{f}_h^{\ell,s} + \epsilon\boldsymbol{y}) - \boldsymbol{g}(\boldsymbol{f}_h^{\ell,s})\right). \tag{3.22}$$

Therefore we can compute the matrix-vector product needed for GMRES, allowing us to iteratively solve for the Newton step in each iteration. This in turn allows the solution of the nonlinear residual (3.13), which completes the definition of the spectral collocation method.

3.3 DG for Hyperbolic Moment Equations

Efficiency concerns with the previous method spurred the investigation of using DG for the globally hyperbolic moment equations introduced in Section 2.3.4. For this section we assume $d = 1$. In expressions that are applicable to both scaling by θ (HME) and scaling by Θ (HMBMM) we by default refer to the scaling parameters as v and Θ, with the understanding that θ can be used interchangeably when needed.

3.3.1 Conservative Form

The starting point for DG methods is a system of conservation laws involving a flux function F as in expression (2.21). Grad's equations (2.19) can be written in conservative form with the change of variables [72]

$$M_i = \frac{1}{i!}\int_{\mathbb{R}} \xi^i f d\xi \tag{3.23}$$

which results in the equations[1]

$$\boldsymbol{u} = \begin{pmatrix} M_0 \\ M_1 \\ \vdots \\ M_{N-1} \end{pmatrix} \; ; \; F(\boldsymbol{u}) = \begin{pmatrix} 1M_1 \\ 2M_2 \\ \vdots \\ NM_N \end{pmatrix} \; ; \; S(\boldsymbol{u}) = \frac{1}{\tau}\begin{pmatrix} \int_{\mathbb{R}^d} \xi^0(\mathcal{M}-f)d\xi \\ \int_{\mathbb{R}^d} \xi^1(\mathcal{M}-f)d\xi \\ \vdots \\ \int_{\mathbb{R}^d} \xi^{N-1}(\mathcal{M}-f)d\xi \end{pmatrix}. \tag{3.24}$$

Recall that Grad's system are not globally hyperbolic. According to the definition of hyperbolicity in Section 2.3.2, this means the eigenvalues of the Jacobian of $F(\boldsymbol{u})$ are not guaranteed to be real.

While HME and HMBMM are globally hyperbolic, they cannot be written in the conservative form of (2.21). The issue arises from the extra term (2.18) subtracted in the last equations of (2.22) and (2.24)

$$\mathcal{F}_N = f_{N-1}\frac{\partial v}{\partial x} + \frac{f_{N-2}}{2}\frac{\partial \Theta}{\partial x} \tag{3.25}$$

These partial derivatives cannot be written as the antiderivative of a flux function. While a nonconservative term can pose complications for standard methods, sacrificing a conservative form for hyperbolicity is a worthy trade here due to the ease of which the nonhyperbolic system can become unstable.

We use the approach used in [10, 58] which uses the same change of variables that puts Grad's equations in conservative form. Due to the similarity in the systems, the

[1]Note that some references including [58, 9] use a change of variables $\widetilde{M}_i = i!M_i$. We found M_i to be more numerically stable for large numbers of moments so the derivations will proceed with this definition

result is a system that is almost conservative; it consists of $N-1$ conservation laws and one equation that cannot be written in conservative form

$$\frac{\partial \boldsymbol{u}}{\partial t} + \frac{\partial F(\boldsymbol{u})}{\partial x} - \mathcal{N}(\boldsymbol{u}, \partial_x \boldsymbol{u}) = S(\boldsymbol{u}) \; ; \; \mathcal{N} = \begin{pmatrix} 0 \\ 0 \\ \vdots \\ N\left(\mathcal{F}_N\right). \end{pmatrix} \tag{3.26}$$

It is worth noting that $\mathcal{F}_N$ involves the coefficient f_{N-1}, which for HMBMM is the constrained coefficient given by (2.25).

3.3.2 Non-conservative Product

Where our method departs from previous attempts is how the nonconservative product is evaluated. Previous approaches have either approximated it with finite differences [14] or used Dal Maso-LeFloch-Murat (DLM) theory for a rigorous treatment involving path-dependent Rankine–Hugoniot conditions [58].

Instead, we move the nonconservative product to the other side of the equation and treat it as part of the source term, giving a modified soure term that depends on $\boldsymbol{u}$ and its gradient

$$L(\boldsymbol{u}, \partial_x \boldsymbol{u}) = S(\boldsymbol{u}) + \mathcal{N}(\boldsymbol{u}, \partial_x \boldsymbol{u}) \tag{3.27}$$

This has been shown to provide satisfactory results for other equations, as long as the derivative is treated in a consistent way in the weak form [62].

3.3.3 Weak Form

While one could directly take the derivative of $\boldsymbol{u}$ by taking the gradient of the basis functions, these functions are not differentiable at the edge between two elements. Instead, we treat the derivatives in the way they typically are in DG methods, by

adding an equation:

$$\frac{\partial \boldsymbol{u}}{\partial t} + \frac{\partial F(\boldsymbol{u})}{\partial x} = L(\boldsymbol{u}, \boldsymbol{q}) \tag{3.28a}$$

$$\frac{\partial \boldsymbol{u}}{\partial x} - \boldsymbol{q} = 0. \tag{3.28b}$$

Then the DG method is defined by finding $(\boldsymbol{u}_h, \boldsymbol{q}_h) \in (\mathcal{W}_h^k, \mathcal{V}_h^k)$ such that for all $(w, \boldsymbol{v}) \in (\mathcal{W}_h^k, \mathcal{V}_h^k)$ the following weak form is satisfied:

$$\left(\frac{\partial \boldsymbol{u}_h}{\partial t}, w\right)_{\mathcal{T}_h} - \left(F(\boldsymbol{u}_h), \frac{\partial w}{\partial x}\right)_{\mathcal{T}_h} + \left\langle \widehat{F}(\boldsymbol{u}_h^+, \boldsymbol{u}_h^-, \boldsymbol{x}), w \right\rangle_{\partial \mathcal{T}_h} = (L(\boldsymbol{u}, \boldsymbol{q}), w)_{\mathcal{T}_h} \tag{3.29a}$$

$$(\boldsymbol{q}_h, \boldsymbol{v})_{\mathcal{T}_h} + \left(\boldsymbol{u}_h, \frac{\partial \boldsymbol{v}}{\partial x}\right)_{\mathcal{T}_h} - \langle \widehat{\boldsymbol{u}_h}, \boldsymbol{v} \cdot \boldsymbol{n} \rangle_{\partial \mathcal{T}_h} = 0 \tag{3.29b}$$

with $\widehat{\boldsymbol{u}_h} = \boldsymbol{u}_h^-$ and $\widehat{F}(\boldsymbol{u}_h^+, \boldsymbol{u}_h^-)$ calculated with a local Lax-Friedrichs flux

$$\widehat{F}(\boldsymbol{u}_h^+, \boldsymbol{u}_h^-, \boldsymbol{x}) = \frac{1}{2}(F(\boldsymbol{u}_h^+) + F(\boldsymbol{u}_h^-)) + \frac{C(\boldsymbol{x})}{2}(\boldsymbol{u}_h^+ - \boldsymbol{u}_h^-) \tag{3.30}$$

where C is the maximum characteristic speed of the system at $\boldsymbol{x}$.

3.3.4 Solution Method

Solving the weak form for $\boldsymbol{u}_h$ leads to the time dependent system

$$\frac{d\boldsymbol{u}_h}{dt} = \boldsymbol{R}(\boldsymbol{u}_h, \boldsymbol{q}_h) \tag{3.31}$$

which is solved with explicit Runge-Kutta time stepping. At each stage in the RK scheme, $\boldsymbol{q}_h$ is calculated by solving the linear system corresponding to (3.29b) and then used in the evaluation of the inner products that make up (3.29a).

The stiffness concern mentioned in Section 3.1.3 is still relevant here, but due to the untested nature of this approach, it was decided to focus on determining whether this method was viable, rather than using an implicit method.

Evaluation of primitive variables, fluxes, and source term

The components of $\boldsymbol{u}_h$ will be referred to as the *conservative variables*. The *primitive variables* will refer to the unknown coefficients in the spectral expansion (2.17).

In order to calculate the residual in (3.31), it is necessary to have mappings between the primitive and conservative variables. Initial conditions are typically expressed in terms of the primitive variables, as are the final quantities of interest. Furthermore, the primitve variables are used in the evaluation of the flux and source terms.

Mapping from primitive to conservative variables can be calculated analytically or numerically using the Hermite expansion:

$$\int_{\mathbb{R}} \xi^i f d\xi = \int_{\mathbb{R}} \xi^i \sum_{\alpha=0}^{N-1} f_\alpha(t,x) \mathcal{H}_\alpha^{v,\Theta}(\xi) d\xi \tag{3.32a}$$

$$= \sum_{\alpha=0}^{N-1} f_\alpha(t,x) \int_{\mathbb{R}} \xi^i H_\alpha^{v,\Theta}(\xi) d\xi. \tag{3.32b}$$

The velocity space integral can be expanded and solved using a change of variables $c = (\xi - v)/\Theta$

$$\int_{\mathbb{R}} \xi^i \mathcal{H}_\alpha^{v,\Theta}(\xi) d\xi = \Theta^{-\alpha/2} \int_{\mathbb{R}} \xi^i He_\alpha\left(\frac{\xi - v}{\sqrt{\Theta}}\right) \frac{1}{\sqrt{2\pi\Theta}} \exp\left(-\frac{|\xi - v|^2}{2\Theta}\right) d\xi \tag{3.33a}$$

$$= \Theta^{-\alpha/2} \int_{\mathbb{R}} \left(c\sqrt{\Theta} + v\right)^i He_\alpha(c) \frac{1}{\sqrt{2\pi}} \exp\left(-\frac{c^2}{2}\right) dc \tag{3.33b}$$

which can be written out exactly using the binomial theorem or solved exactly using Gauss-Hermite quadrature [20].

Going from the conservative to primitive variables is less straightforward. First we need expressions for the scaling parameters v and Θ:

$$v = \frac{M_1}{M_0} \tag{3.34}$$

$$\Theta^{\frac{N-1}{2}} = \frac{1}{(N-2)!!\rho}\int_{\mathbb{R}}(\xi - v)^{N-1} f(t,x,\xi)d\xi \tag{3.35a}$$

$$= \frac{1}{(N-2)!!\rho}\int_{\mathbb{R}}\sum_{k=0}^{N-1}\binom{N-1}{k}\xi^k(-1)^{N-1-k}v^{N-1-k}f(t,x,\xi)d\xi \tag{3.35b}$$

$$= \frac{1}{(N-2)!!\rho}\sum_{k=0}^{N-1}\binom{N-1}{k}(-1)^{N-1-k}v^{N-1-k}k!M_k. \tag{3.35c}$$

In particular for the 3rd centered moment used for rescaling in HME:

$$\theta = \frac{1}{\rho}\left(2M_2 - 2vM_1 + v^2M_0\right) \tag{3.36a}$$

$$= \frac{1}{M_0}\left(2M_2 - 2\frac{M_1^2}{M_0} + \left(\frac{M_1}{M_0}\right)^2 M_0\right) \tag{3.36b}$$

$$= \frac{2M_2}{M_0} - v^2. \tag{3.36c}$$

The mapping from conservative to primitive variables is complete by using the expression derived in [15]:

$$f_\alpha = \sum_{k=0}^{\alpha}(-1)^{(\alpha-k)}\frac{He_{\alpha-k}(v/\sqrt{\Theta})}{(\alpha-k)!}\Theta^{\left(\frac{\alpha-k}{2}\right)}M_k. \tag{3.37}$$

The numerical flux function involves known quantities $M_1, \ldots, M_{N-1}$ and an unknown M_N. To calculate M_N we map from the known conservative values $\boldsymbol{u}_h$ to primitive variables and use (3.32) and (3.33b). The primitive variables calculated for the flux evaluation are reused for the source term evaluation. All source term components contain

$$\int_{\mathbb{R}}\xi^i(\mathcal{M}(f) - f)d\xi = \int_{\mathbb{R}}\xi^i\mathcal{M}(f)d\xi - M_i \tag{3.38}$$

with the first integral exactly calculable with quadrature or analytically. To evaluate the source term, it remains to calculate the nonconservative product (3.25).

For the nonconservative product now in the last component of the source term, we need to evaluate $\partial_x v$ and $\partial_x\theta$ or $\partial_x\Theta$, depending on the scaling used. We can

assume we have access to the approximate solution $\boldsymbol{u}_h$ and the approximation to its derivative $\boldsymbol{q}_h$. Since we have expressions for v (3.34), θ (3.36), and Θ (3.35), in terms of the components of $\boldsymbol{u}_h$, we can get expressions for their derivatives. Specifically, these expressions are

$$\frac{\partial v}{\partial x} = \frac{M_0 q_1 - M_1 q_0}{M_0^2} \tag{3.39}$$

$$\frac{\partial \theta}{\partial x} = 2\frac{M_0 q_2 - M_2 q_0}{M_0^2} - 2v\frac{\partial v}{\partial x} \tag{3.40}$$

$$\frac{\partial \Theta}{\partial x} = \frac{2}{2(N-1)(N!!)}\Theta^{(3-N)/2}\left(A_{N-1} + \sum_{k=0}^{N-2}(A_K + B_k)\right) \tag{3.41}$$

with

$$A_k = \frac{(N-1)!}{(N-k-1)!}\left((-v)^{N-1-k}\frac{M_0 q_k - M_k q_0}{M_0^2}\right) \tag{3.42a}$$

$$B_k = -\frac{(N-1)!}{(N-k-2)!}\left((-v)^{N-2-k}\frac{M_k}{M_0}\frac{\partial v}{\partial x}\right). \tag{3.42b}$$

With the ability to evaluate $\boldsymbol{R}(\boldsymbol{u}_h, \boldsymbol{q}_h)$, we can proceed by using the explicit Runge-Kutta methods described in Section 3.1.3 to evolve the system in time.

Chapter 4

Numerical Results

This chapter includes numerical results for both methods. The spectral collocation method is tested on 1D and 2D problems and later used as a reference solution for the DG moment methods. The DG moment methods have their convergence validated and are demonstrated on a common shock tube problem in varying physical regimes.

4.1 Reference Implicit DG Solver

4.1.1 Smooth Problem

The first test case is adapted from [68] and is used here for demonstrating convergence. The spatial and velocity domains are one-dimensional and the initial distribution is smooth and varying in space:

$$f(x,v,0) = \frac{\rho}{\sqrt{2\pi T}}\exp\left(-\frac{(v-u_0(x))^2}{2T}\right), x \in [-1,1]$$
$$u_0(x) = \frac{1}{10}\left(\exp\left(-\left(10x-1\right)^2\right)\right) - 2\exp\left(-\left(10x+3\right)^2\right)\Big).$$

To measure convergence, we calculate a reference solution with 512 uniform elements in space and degree 4 basis functions. The velocity space uses a single element with a degree 23 spectral and the solution is advanced until $t = 0.04$ with an L-stable

p Order	ρ	v	θ
1	1.7033	1.7788	1.7477
2	3.0455	2.8105	3.0760
3	3.9621	3.7828	3.8997
4	4.9024	4.7915	4.8006

Table 4.1: Order $p+1$ rates of L_2 convergence for reference implicit DG method on smooth problem

DIRK(3,3) method. The very high order of the velocity space approximation is viable with this specific choice of basis and is chosen so that the error in velocity space is negligible. See Figure 4-1 and table 4.1.1 for $p+1$ order convergence.

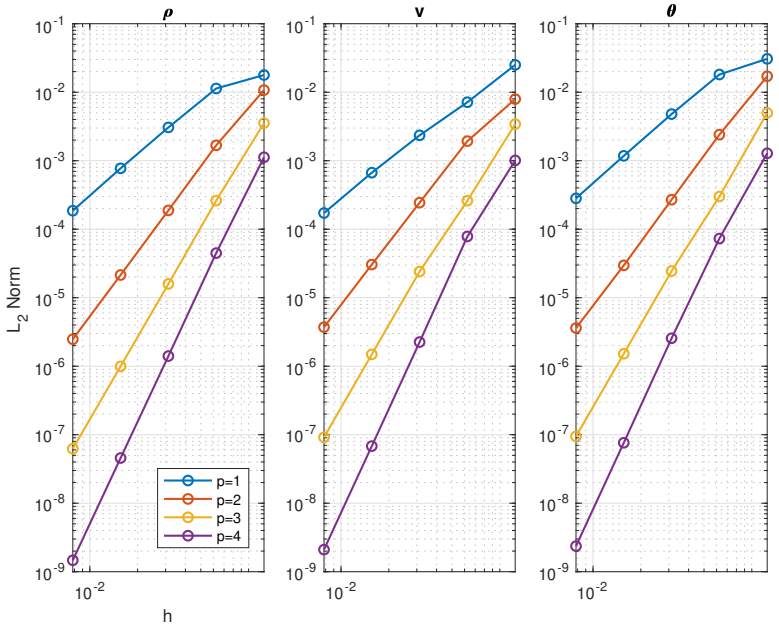

Figure 4-1: Convergence in moments for implicit DG method

4.1.2 2D Problem

This method was run on a number of other standard 1D benchmarks, but its flaws weren't apparent until a 2D problem was attempted. For 2D problems, it was found that the sweeping preconditioner was not scaling well enough to be viable in its current form. Relatively modest 2D problems, for example with around 90^2 and 50^2

degrees of freedom in physical and velocity space respectively, were found to already computationally expensive, with the sample in Figure 4-2 taking almost an hour on 64 processors on the MIT SuperCloud cluster using MPI parallelization [71]. With the use of the BGK collision operator, this is just not competitive with other similar solvers.

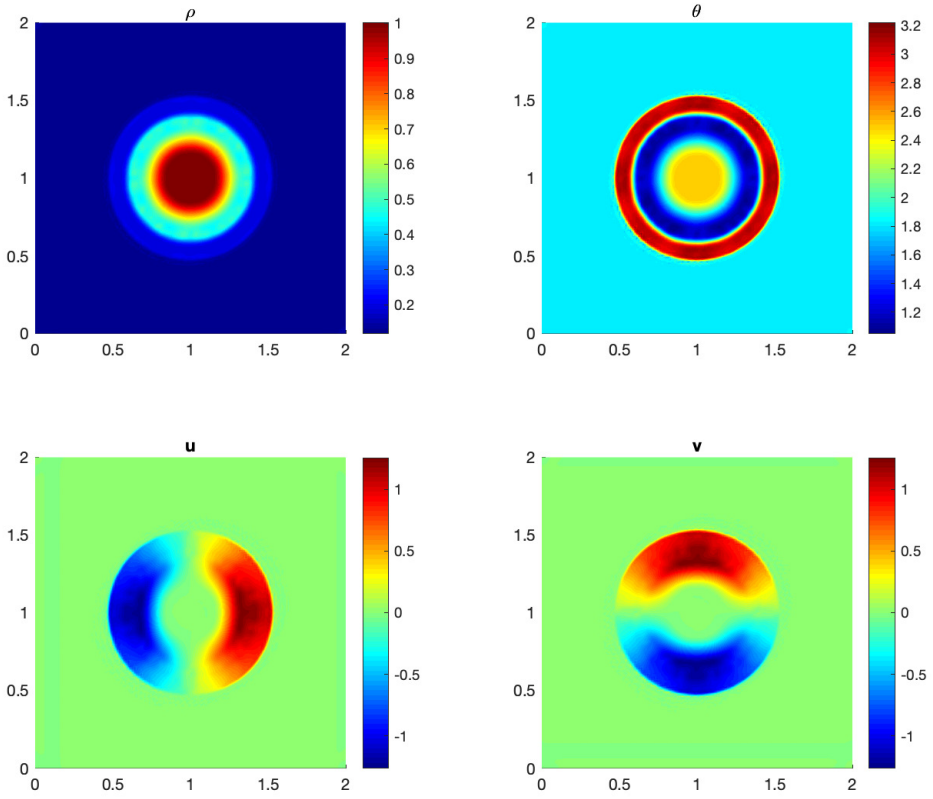

Figure 4-2: Macroscopic moments for a 2D Riemann problem using a 100x100 spatial grid and degree 2 basis functions with a velocity space of 30^2 collocation points.

4.2 Hyperbolic Moment Models

4.2.1 Smooth Problem

We now use the moment models on the same smooth problem from Section 4.1.1. Our method should perform well for this problem due to the spectral accuracy of the

Hermite polynomial basis. Similarly, with a high order DG discretization in physical space, we can use relatively few elements in space. While not too challenging of a problem on its own, it allows us to validate our approach and measure its convergence. The spectral collocation method is used as a reference solution.

To check that the approximation in velocity space is converging, we start with a 4th-order spatial approximation with 300 elements and a small time step with RK4 time stepping so that the errors in space and time are negligible. As shown in Figure 4-3, the solutions coincide visually with just 5 basis functions. Increasing the number of basis functions does not pollute the solution. In fact, Figure 4-4 shows the absolute error of the moment method and the reference method decrease as more basis functions are added. The case with 5 equations is already quite close to the reference solution, and adding more equations improves the approximation.

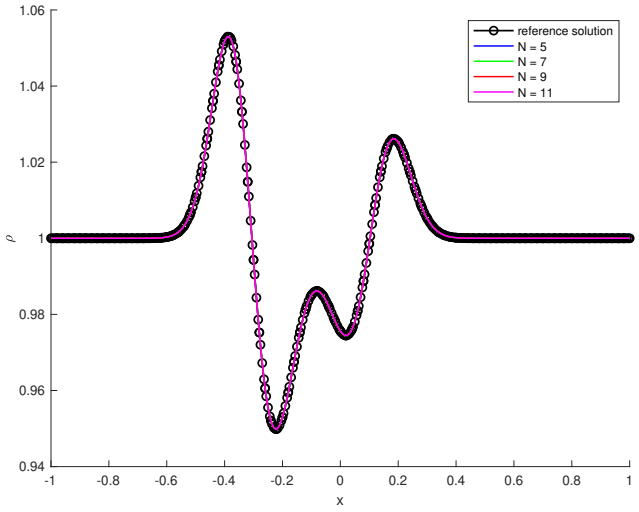

Figure 4-3: Density for smooth initial conditions

To check spatial convergence, we set $N = 11$ and compare HME and HMBMM results against the reference solution. See Figure 4-5 for convergence plots of ρ, v, and θ and table 4.2.1 for the rates. For $p = 3$ and $p = 4$ the error flattens out somewhat for the finest meshes; at these small magnitudes (a squared L^2 error of 1e-13), the solution could be polluted by time-stepping or velocity-space approximation error. Note that the errors for the two models are indistinguishable. This shows the

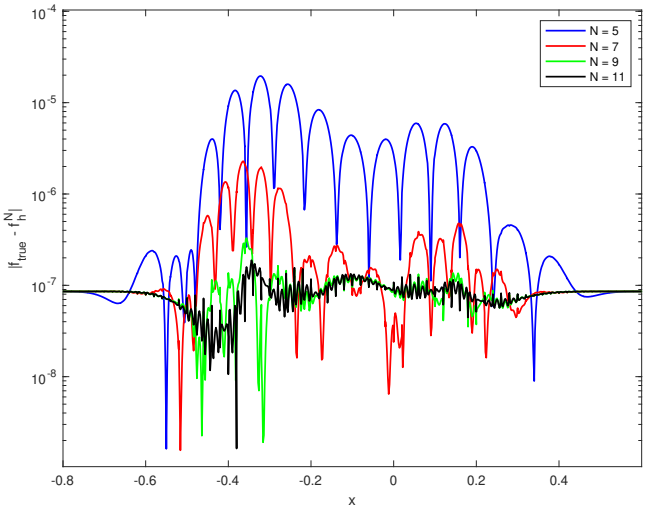

Figure 4-4: As the number of equations is increased, the maximum error decreases

approximation in velocity space is independent of scaling strategy as long as enough basis functions are used.

p Order	ρ	v	θ
1	1.7546	1.9058	1.7864
2	2.5173	2.5652	3.0055
3	3.9791	3.8694	3.8358
4	4.9112	4.9140	4.6546

Table 4.2: Rates of convergence for HMBMM show rates between $p + 1/2$ and $p + 1$. Nearly identical rates are found for HME

4.2.2 Riemann Problem

The second example is a standard benchmark for moment methods. It is a Riemann problem on the domain [-2,2] with states on either side of the origin:

$$f(x, v, 0) = \begin{cases} \frac{\rho_L}{\sqrt{2\pi\theta_L}} \exp\left(-\frac{v_L^2}{2\theta_L}\right), x \in [-2, 0) \\ \frac{\rho_R}{\sqrt{2\pi\theta_R}} \exp\left(-\frac{v_R^2}{2\theta_R}\right), x \in [0, 2] \end{cases} \tag{4.1}$$

with $(\rho_L, v_L, \theta_L) = (7, 0, 1)$ and $(\rho_R, v_R, \theta_R) = (1, 0, 1)$

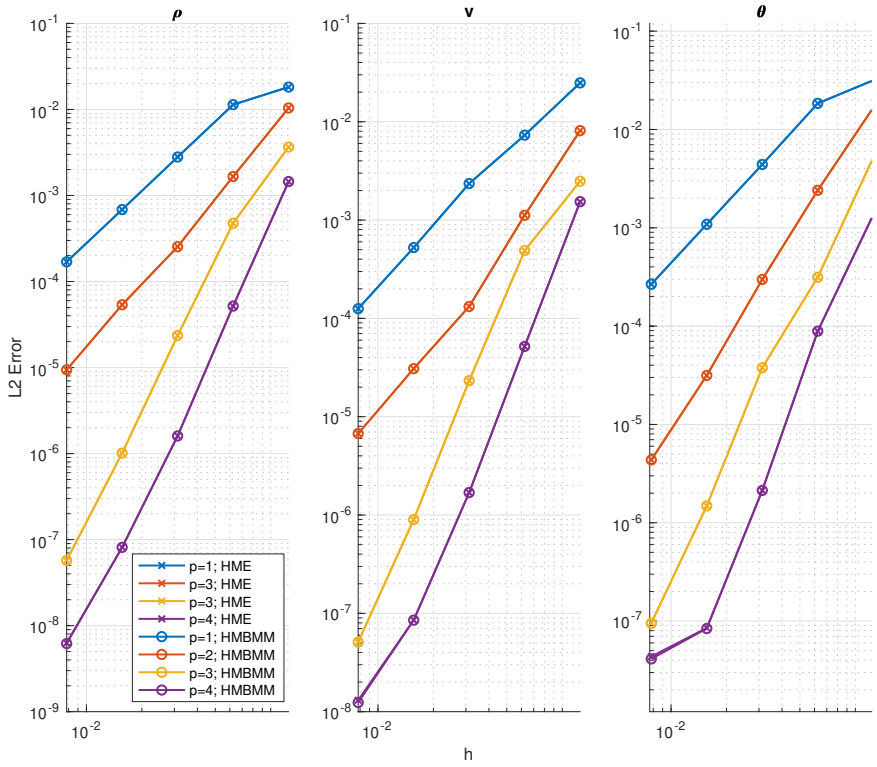

Figure 4-5: Convergence in L_2 norm for macroscopic quantities for the DG hyperbolic moment models. HMBMM and HME results are indistinguishable

Discontinuities like this are a known challenge for DG. Usually the discontinuity is handled with shock capturing of some form, for example with limiters or artificial viscosity. For now, we sidestep this concern by replacing the discontinuity in the initial condition with a fitted smooth function, in this case a hyperbolic tangent function. Comparisons to results in the literature confirm that this does not have a discernable effect on the final result.

These simple initial conditions can introduce significant nonequilibrium effects depending on the relaxation time. For this reason we focus on the behavior of the solution for different values of τ. For all examples below, the relaxation time τ is defined as Kn/ρ and is therefore a function of space. The results are shown at $t = 0.3$.

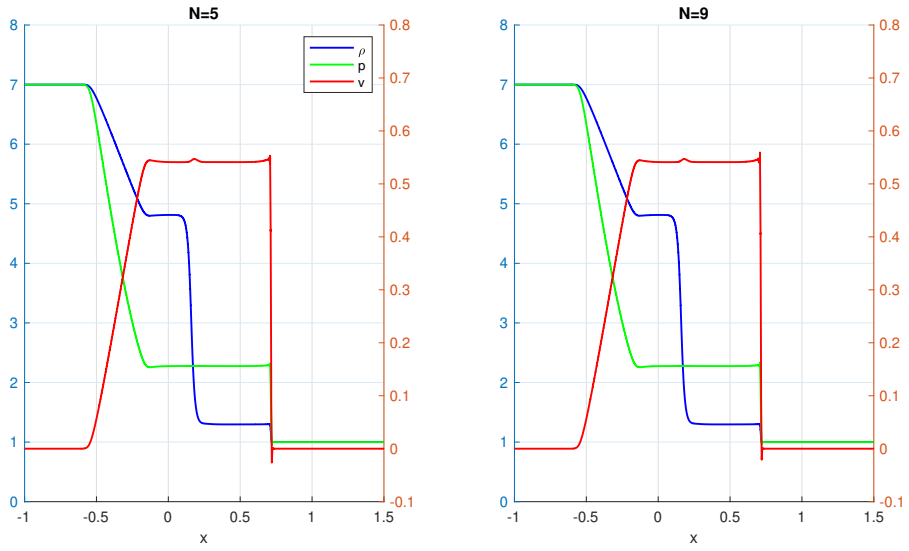

Figure 4-6: Kn=1e-4 results approximate approach the Euler solution

Fluid Regime

We begin close to the fluid regime, with Kn=5e-4. In this case, the rescaling should be particularly effective. Figure 4-6 confirms this is the case. We see that $N = 5$ and $N = 9$ give similar results. This means that five basis functions in velocity space is sufficient to capture the distributions that are expected to be near-Maxwellian everywhere. Note that there are some slight oscillations around $x = 0.7$, likely a result of the sharp gradient in the solution.

One issue worth noting is the time step; as the Knudsen number decreases, the source term becomes more stiff and a smaller time-step is required as mentioned in Section 3.1.3.

Transitional Regime

For moderate nonequilibrium we increase the Knudsen number to 5e-2. We fix a spatial discretization of 300 uniform elements and $p = 2$ basis functions. See Figure 4-7 for examples with increasing N. Now, the solution smooths out as we increase N, with near identical results for $N = 9$ and $N = 11$, indicating convergence in velocity space. The profile of the solution agrees with results in [58], which compares a few

different moment methods, including HME.

As we increase the degree of nonequilibrium, the nonconservative product in the last equation becomes more relevant. see Figure 4-8 for an example of its impact on the final solution.

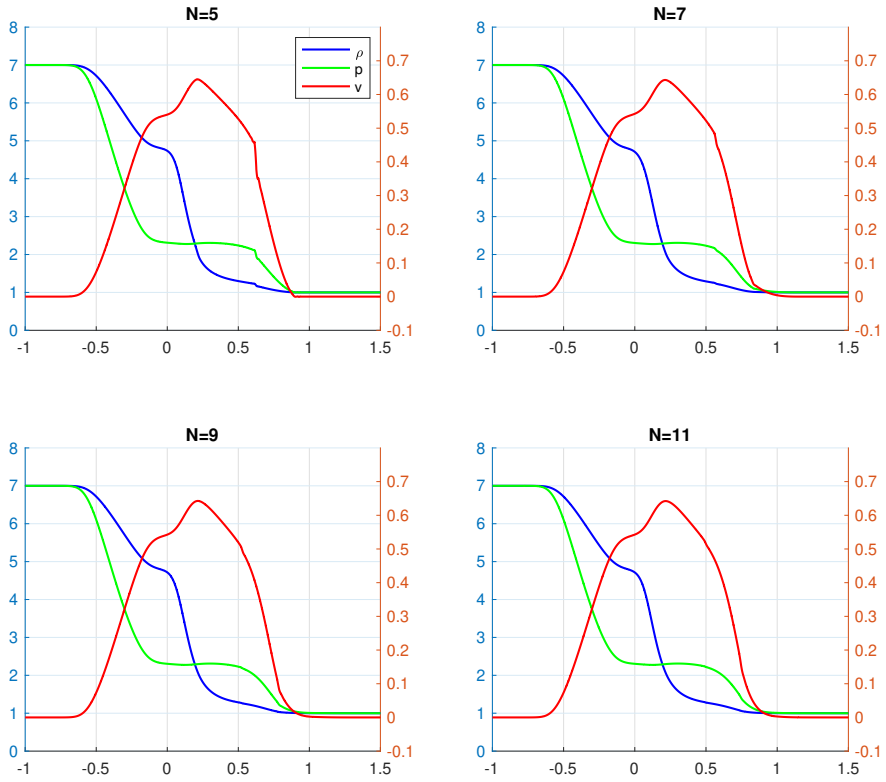

Figure 4-7: Standard Riemann problem. As the number of equations is increased, the solution smooths out

Kinetic Regime

Finally we increase Kn to 5e-1. Previous tests for this problem see unphysical subshocks, which appear as a staircase-like pattern in front of the shock.

As noted in [9], the Θ-scaling of HMBMM will not resolve the subshock issue. We can see in Figure 4-9 that both HME and HMBMM behave in similar ways. The pattern and number of steps coincides with the number of basis functions, but the locations and size of the subshocks differ. This is likely due to the fact that the two

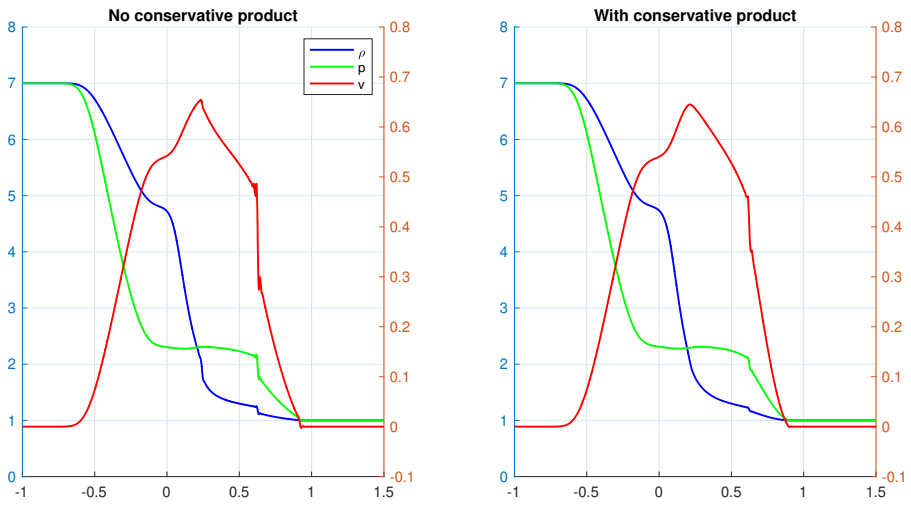

Figure 4-8: Left is the solution with out the nonconservative product in the last equation, right has it included. It has a small smoothing effect

methods have different characteristic speeds. This can be seen more clearly in Figure 4-10, which overlays HMBMM and HME results for $N = 13$. Due to the hyperbolic correction, we can increase the number of polynomials in velocity space. In theory, we can increase N arbitrarily, but in practice numerical difficulties can occur.

This is particularly the case for HMBMM. The definition of Θ leaves little room for error. Despite greatly increasing the spatial and temporal resolution, using HMBMM with 15 polynomials would regularly become unstable due to the appearance of a negative Θ. At first, this seemed to be a failure of the handling of the nonconservative term. While this could be the case, the implementation has the desired effect for HME and appears to be correct for HMBMM with smaller N. In fact, as N increases, Θ can become negative if the distribution f is even slightly negative. See Figure 4-11 for an example of this. At the same time, the HMBMM results are better quality than the corresponding HME results. It seems that using Θ is a more effective scaling but is much more sensitive. Therefore it appears to have stricter requirements on grid and time-step size than the θ scaling of HME and the handling of discontinuities is likely even more important than for HME.

Convergence in velocity space is very slow as shown in Figure 4-12. This is a known

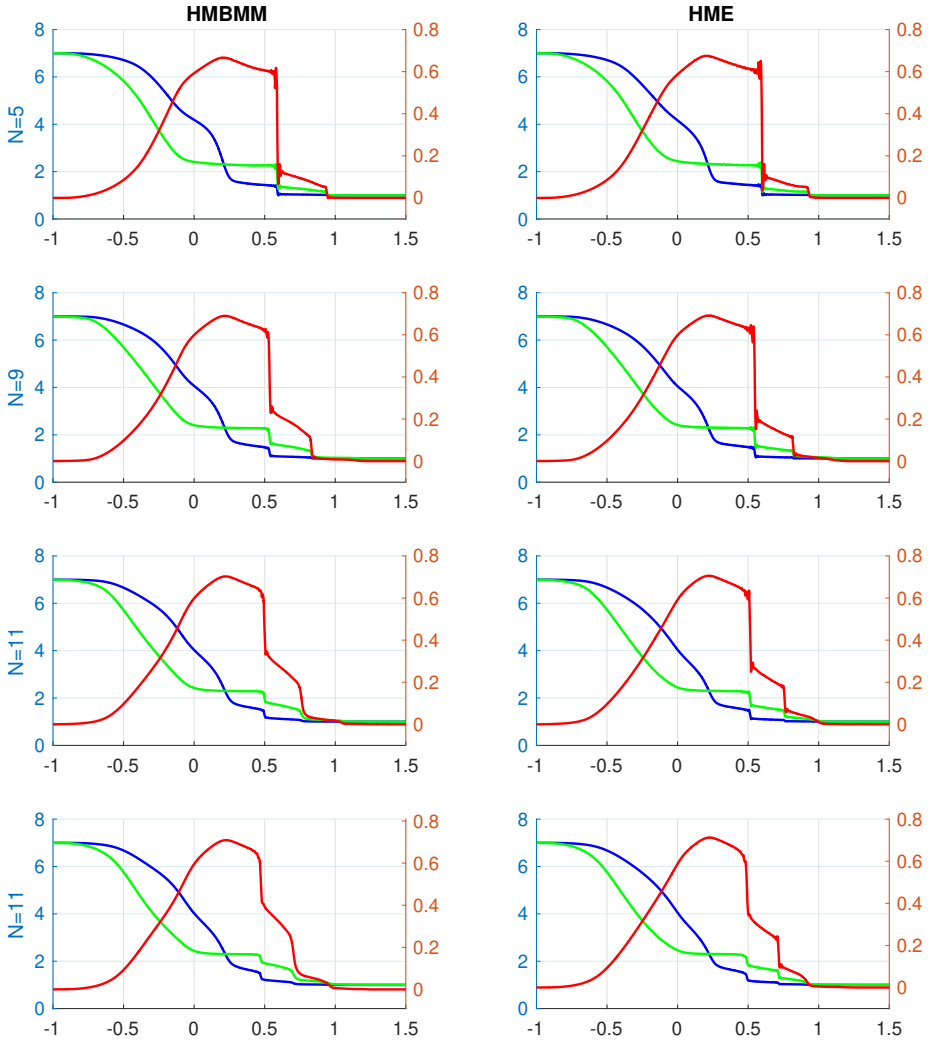

Figure 4-9: Gradual convergence for the discontinuous problem. HMBMM seems to be of better quality, though there is a practical limit to how large N can grow for it. After $N = 13$, we find it difficult to avoid negative Θ

issue and it has to do with the distribution function f in this problem. Figure 4-13 compares the calculated distribution from HME to a reference distribution calculated with the spectral collocation method with a very fine velocity space approximation. The true solution approaches a discontinuous function and, as N is increased, the spectral approximation exhibits oscillations, a consequence of the Gibbs phenomenon.

An advantage of the moment methods is that they provide a rigorous framework for

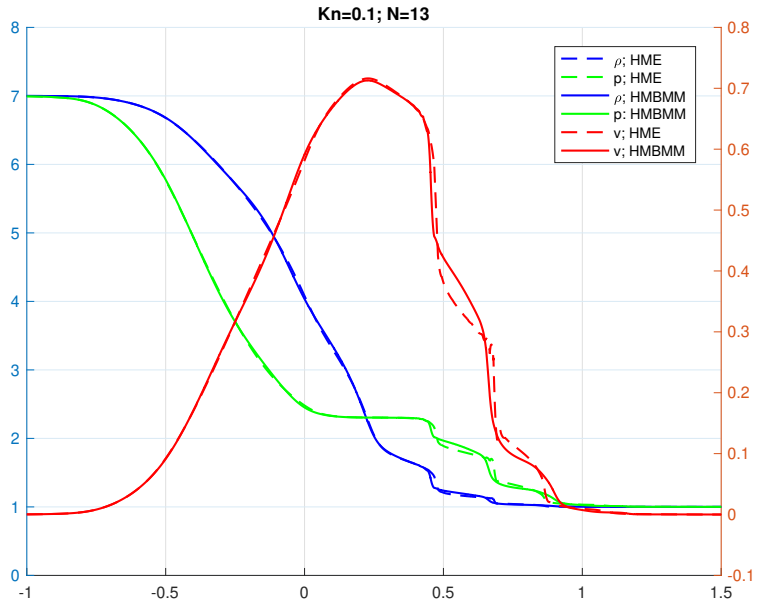

Figure 4-10: More direct comparison of the subshock patterns for HME and HMBMM. While the general behavior is similar, the exact structure of the subshocks is noticeably different between the two methods.

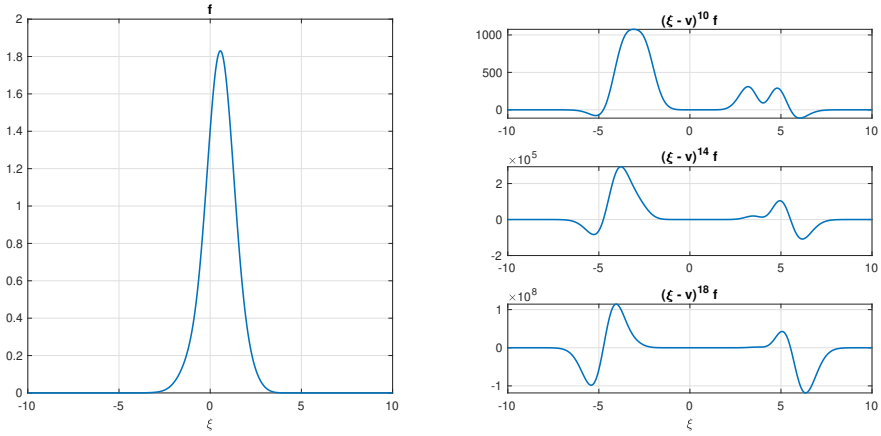

Figure 4-11: An example of the sensitivity of Θ for large N. On the left is distribution that appears in our simulation of the Riemann problem with Kn $= 0.5$. On the right is the function $g(\xi) = (\xi - v)^{N-1} f$ for increasing values of N. The distribution is slightly negative (5e-6) at two regions; this slight negativity can lead to $\int g(\xi) d\xi$ being negative for large enough N. By (2.23), this leads to negative or imaginary Θ.

addressing this issue. These discontinuous distributions can occur in shock problems and at solid boundaries with reflective boundary conditions, so it's not a problem that

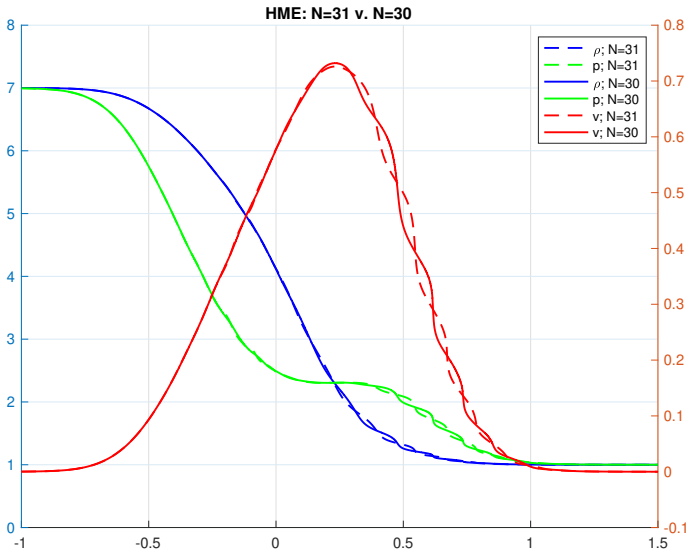

Figure 4-12: Riemann problem using HME with very high N. Despite the very high order, convergence is slow

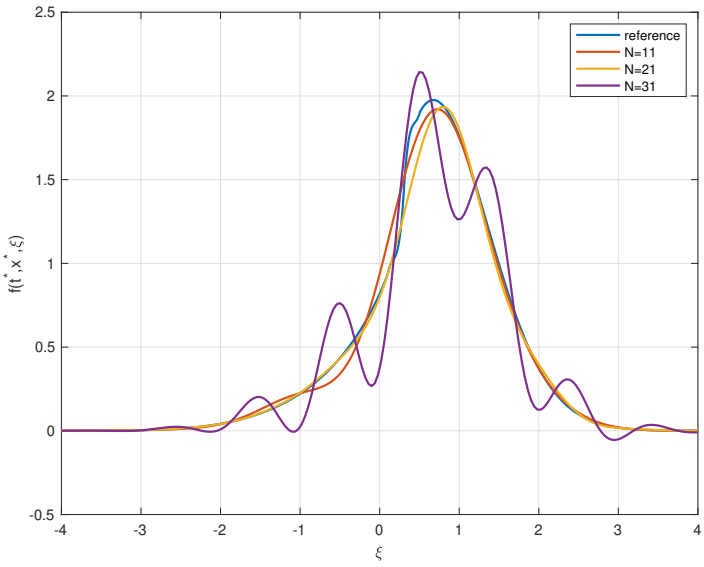

Figure 4-13: f at a fixed $t^* = 0.3$ and $x^* = 0.1$ for the Riemann problem with $\mathrm{Kn} = 0.5$. A reference f, computed with the implicit DG method, has a steep jump around the origin. Oscillations occur as we try to use higher order spectral bases, slowing down the convergence in velocity space.

can be ignored. But it can be addressed with alternate basis functions like splines [57] or methods like filtering that improve the convergence of spectral methods [29].

These approaches will be important for a robust DG solution for hyperbolic moment equations and HMBMM in particular. First, high spatial accuracy is wasted if the velocity space is underresolved. Second, the subshocks that appear in this case can easily cause instabilities for DG. To avoid the oscillations that can be particularly problematic for HMBMM, a careful treatment of discontinuous distributions is likely essential.

Chapter 5

Future directions

This thesis explored two novel DG methods for the Boltzmann equation. The first method, a spectral collocation approach, aimed to combine the simplicity of having equations corresponding to discrete velocities, with the flexibility and expressivity of a spectral velocity space basis. Implicit time integration was used with an iterative method and sweeping preconditioner. Examples were shown in 1D and 2D to investigate the method's efficiency. The second approach used DG for globally hyperbolic moment equations. The focus here was to validate that this method could work with these equations, so it was tested on common 1D problems. This chapter focuses on the ramifications of our results and promising directions for future research.

5.1 Spectral Collocation

While this particular method was validated and could conceivably be made viable for slightly rarefied low speed flows, it was not successful enough to encourage further development in its current form. In 2D, the preconditioner was found to be inefficient and exhibited poor scalability. The nodal polynomial basis adds cost and complicates extensions to reflective boundary conditions, while losing the benefits of fast spectral methods for the full collision operator. An area where this approach could be effective is to allow for adaptive basis functions, but this particular sweeping preconditioner requires a uniform velocity space treatment everywhere. While the sweeping order

could be recalculated to allow for adaptation in time, spatial adaptivity is not an obvious extension.

Still, there is interest in developing high order solvers for the Boltzmann equation. Our experience shows that success for realistic problems depends greatly on how the velocity space is described. It should either be constructed to allow for efficient collision operator evaluations [45, 76, 23] or adaptation to macroscopic features in space and time [52, 77]. A spectral collocation method that can accomplish this, for example with more deliberate choices of basis functions or the ability to vary the collocation nodes across space and time, could be an effective method.

5.2 DG for Moment Models

Using DG for the hyperbolic moment equations seems promising enough to warrant further investigation. The strategy of moving the nonconservative product to the source term appears to successfully stabilize the system even for large numbers of moments, in particular for HME. In addition to the obvious extensions to higher dimensions and different test cases, future work should focus on improving efficiency and robustness.

5.2.1 Future work

There are recent improvements to moment methods that could be implemented here, like alternative basis choices [57, 40] and Asymptotic-Preserving schemes tailored to these models that avoid the CFL restriction [56].

The locality inherent in the approximation spaces of DG allows for h-p adaptivity, where the mesh and polynomial order are adjusted to local solution features. This would also make DG a natural method with which to implement moment- or m-adaptivity, where the resolution in velocity space is adjusted based on a local measure of nonequilibrium. This has been attempted with different moment models [2] and HME with a first-order finite volume method [54]. This approach would allow for a high-order adaptive method and could even accommodate h-p-m adaptivity.

The biggest challenge for applying DG to moment methods appears to be robustness in the presence of velocity-space underresolution. Discontinuous distributions can occur in rarefied conditions with standard Riemann problems and reflective boundary conditions. While the hyperbolic fix allows for an arbitrary number of velocity space basis functions, there is a practical limit to how many can be used, especially in 2 or 3 dimensions. The unphysical subshocks that form as a result of the discontinuous distribution can lead to oscillations that are particularly problematic for the numerically sensitive Θ scaling. Anything that can be done to mitigate this issue should be used with a DG implementation. A promising approach is the use of spectral filters, as proposed in [29]. The interpretation of these filters as artificial collisions could serve as a guide for the construction of other artificial source terms, which have proven successful with DG methods [67]. The artificial Knudsen number method used in [83] could also be helpful.

A useful application of this method could be in a hybrid solver, like [34]. In this method, Navier-Stokes and Boltzmann solvers are coupled. The moment methods could be an effective bridge between these models. The globally hyperbolic moment methods could be used in regimes of moderate nonequilibrium, reducing the use of an expensive Boltzmann solver. At the same time, use of the method in regions where unphysical subshocks might appear would be limited. This is another form of model adaptivity abetted by using DG, where the fluid and kinetic regimes solve different PDEs entirely. The fact that these methods are high-order in space would allow the development of a uniformly high-order hybrid method.

Bibliography

[1] MRA Abdelmalik and EH van Brummelen. An entropy stable discontinuous galerkin finite-element moment method for the boltzmann equation. *Computers & Mathematics with Applications*, 72(8):1988–1999, 2016.

[2] MRA Abdelmalik and EH van Brummelen. Error estimation and adaptive moment hierarchies for goal-oriented approximations of the boltzmann equation. *Computer Methods in Applied Mechanics and Engineering*, 325:219–239, 2017.

[3] Céline Baranger, Jean Claudel, Nicolas Hérouard, and Luc Mieussens. Locally refined discrete velocity grids for stationary rarefied flow simulations. *Journal of Computational Physics*, 257:572–593, January 2014. arXiv: 1304.5611.

[4] Florian Bernard, Angelo Iollo, and Gabriella Puppo. A Local Velocity Grid Approach for BGK Equation. *Communications in Computational Physics*, 16(4):956–982, October 2014.

[5] P. L. Bhatnagar, E. P. Gross, and M. Krook. A Model for Collision Processes in Gases. I. Small Amplitude Processes in Charged and Neutral One-Component Systems. *Physical Review*, 94(3):511–525, May 1954.

[6] G.A. Bird. *Molecular Gas Dynamics and the Direct Simulation of Gas Flows*. Number v. 1 in Molecular Gas Dynamics and the Direct Simulation of Gas Flows. Clarendon Press, 1994.

[7] Niclas Böhmer and Manuel Torrilhon. Entropic quadrature for moment approximations of the boltzmann-bgk equation. *Journal of Computational Physics*, 401:108992, 2020.

[8] Walter Boscheri and Giacomo Dimarco. High order finite volume schemes with imex time stepping for the boltzmann model on unstructured meshes. *arXiv preprint arXiv:2103.14890*, 2021.

[9] Zhenning Cai. Bridging hydrodynamics and kinetic theory: Challenge from shock structure problems. *arXiv:2006.11115 [physics]*, June 2020. arXiv: 2006.11115.

[10] Zhenning Cai, Yuwei Fan, and Ruo Li. Globally hyperbolic regularization of grad's moment system in one dimensional space. *arXiv preprint arXiv:1111.3409*, 2011.

[11] Zhenning Cai, Yuwei Fan, and Ruo Li. A Framework on Moment Model Reduction for Kinetic Equation. *arXiv:1402.0653 [math-ph]*, February 2014. arXiv: 1402.0653.

[12] Zhenning Cai, Yuwei Fan, and Ruo Li. Globally hyperbolic regularization of grad's moment system. *Communications on pure and applied mathematics*, 67(3):464–518, 2014.

[13] Zhenning Cai, Yuwei Fan, and Ruo Li. On hyperbolicity of 13-moment system. *arXiv preprint arXiv:1401.7523*, 2014.

[14] Zhenning Cai, Yuwei Fan, and Ruo Li. Hyperbolic model reduction for kinetic equations. *arXiv preprint arXiv:2001.10370*, 2020.

[15] Zhenning Cai, Yuwei Fan, Ruo Li, and Zhonghua Qiao. Dimension-reduced hyperbolic moment method for the boltzmann equation with bgk-type collision. *Communications in Computational Physics*, 15(5):1368–1406, 2014.

[16] Zhenning Cai and Manuel Torrilhon. On the holway-weiss debate: Convergence of the grad-moment-expansion in kinetic gas theory. *Physics of Fluids*, 31(12):126105, 2019.

[17] Zhenning Cai and Yanli Wang. Numerical solver for the boltzmann equation with self-adaptive collision operators. *arXiv preprint arXiv:2102.08559*, 2021.

[18] C. Cercignani and C. Michaelis. Rarefied Gas Dynamics: From Basic Concepts to Actual Calculations. Cambridge Texts in Applied Mathematics. *Applied Mechanics Reviews*, 54(5):B90, January 2001.

[19] Songze Chen. Quadrature with equilibrium offset and its application on adaptive velocity grid. page 060003, Glasgow, UK, 2019.

[20] Peter Deuflhard and Andreas Hohmann. *Numerical analysis in modern scientific computing: an introduction*, volume 43. Springer Science & Business Media, 2012.

[21] Yana Di, Yuwei Fan, and Ruo Li. 13-moment system with global hyperbolicity for quantum gas. *Journal of Statistical Physics*, 167(5):1280–1302, 2017.

[22] G. Dimarco and L. Pareschi. Numerical methods for kinetic equations. *Acta Numerica*, 23:369–520, May 2014.

[23] Giacomo Dimarco and Raphael Loubere. Towards an ultra efficient kinetic scheme. Part II: The high order case. *Journal of Computational Physics*, 255:699–719, December 2013.

[24] Giacomo Dimarco and Raphaël Loubere. Towards an ultra efficient kinetic scheme. Part I: Basics on the BGK equation. *Journal of Computational Physics*, 255:680–698, December 2013.

[25] Giacomo Dimarco, Raphaël Loubère, Jacek Narski, and Thomas Rey. An efficient numerical method for solving the Boltzmann equation in multidimensions. *Journal of Computational Physics*, 353:46–81, January 2018.

[26] Giacomo Dimarco and Lorenzo Pareschi. Asymptotic Preserving Implicit-Explicit Runge–Kutta Methods for Nonlinear Kinetic Equations. *SIAM Journal on Numerical Analysis*, 51(2):1064–1087, January 2013.

[27] Junming Duan, Yangyu Kuang, and Huazhong Tang. Model reduction of a kinetic swarming model by operator projection. *arXiv preprint arXiv:1701.02888*, 2017.

[28] Ben Evans, Ken Morgan, and Oubay Hassan. A discontinuous finite element solution of the Boltzmann kinetic equation in collisionless and BGK forms for macroscopic gas flows. *Applied Mathematical Modelling*, 35(3):996–1015, March 2011.

[29] Yuwei Fan and Julian Koellermeier. Accelerating the convergence of the moment method for the boltzmann equation using filters. *Journal of Scientific Computing*, 84(1):1–28, 2020.

[30] Yuwei Fan, Julian Koellermeier, Jun Li, Ruo Li, and Manuel Torrilhon. Model Reduction of Kinetic Equations by Operator Projection. *Journal of Statistical Physics*, 162(2):457–486, January 2016. arXiv: 1412.7296.

[31] Yuwei Fan and Ruo Li. Globally hyperbolic moment system by generalized hermite expansion. *arXiv preprint arXiv:1401.4639*, 2014.

[32] Francis Filbet, Clément Mouhot, and Lorenzo Pareschi. Solving the Boltzmann Equation in $N \log_2 N$. *SIAM Journal on Scientific Computing*, 28(3):1029–1053, January 2006.

[33] Francis Filbet and Thomas Rey. A Rescaling Velocity Method for Dissipative Kinetic Equations - Applications to Granular Media. *Journal of Computational Physics*, 248:177–199, September 2013. arXiv: 1204.5275.

[34] Francis Filbet and Tao Xiong. A hybrid discontinuous galerkin scheme for multiscale kinetic equations. *Journal of Computational Physics*, 372:841–863, 2018.

[35] Rodney O Fox. Higher-order quadrature-based moment methods for kinetic equations. *Journal of Computational Physics*, 228(20):7771–7791, 2009.

[36] Irene M. Gamba, Jeffrey R. Haack, Cory D. Hauck, and Jingwei Hu. A Fast Spectral Method for the Boltzmann Collision Operator with General Collision Kernels. *SIAM Journal on Scientific Computing*, 39(4):B658–B674, January 2017.

[37] Irene M Gamba and Sergej Rjasanow. Galerkin–petrov approach for the boltzmann equation. *Journal of Computational Physics*, 366:341–365, 2018.

[38] Gian Pietro Ghiroldi and Livio Gibelli. A direct method for the boltzmann equation based on a pseudo-spectral velocity space discretization. *Journal of Computational Physics*, 258:568–584, 2014.

[39] Harold Grad. On the kinetic theory of rarefied gases. *Communications on pure and applied mathematics*, 2(4):331–407, 1949.

[40] Jiequn Han, Chao Ma, Zheng Ma, and Weinan E. Uniformly Accurate Machine Learning Based Hydrodynamic Models for Kinetic Equations. *Proceedings of the National Academy of Sciences*, 116(44):21983–21991, October 2019. arXiv: 1907.03937.

[41] Jingwei Hu, Jie Shen, and Yingwei Wang. A petrov-galerkin spectral method for the inelastic boltzmann equation using mapped chebyshev functions. *Kinetic & Related Models*, 13(4), 2020.

[42] Zhicheng Hu and Zhenning Cai. Burnett spectral method for high-speed rarefied gas flows. *SIAM Journal on Scientific Computing*, 42(5):B1193–B1226, 2020.

[43] Zhicheng Hu, Zhenning Cai, and Yanli Wang. Numerical simulation of microflows using hermite spectral methods. *SIAM Journal on Scientific Computing*, 42(1):B105–B134, 2020.

[44] Shashank Jaiswal, Alina A. Alexeenko, and Jingwei Hu. A Discontinuous Galerkin Fast Spectral Method for the Full Boltzmann Equation with General Collision Kernels. *Journal of Computational Physics*, 378:178–208, February 2019. arXiv: 1809.10186.

[45] Shashank Jaiswal, Jingwei Hu, and Alina A. Alexeenko. Fast deterministic solution of the full Boltzmann equation on graphics processing units. page 060001, Glasgow, UK, 2019.

[46] Shi Jin. Asymptotic preserving (ap) schemes for multiscale kinetic and hyperbolic equations: a review. *Rivista di Matematica della Università di Parma. New Series*, 2, 01 2010.

[47] Eswar Josyula, editor. *Hypersonic Nonequilibrium Flows: Fundamentals and Recent Advances*. American Institute of Aeronautics and Astronautics, Inc., Reston, VA, January 2015.

[48] A. Karakus, N. Chalmers, J.S. Hesthaven, and T. Warburton. Discontinuous Galerkin discretizations of the Boltzmann–BGK equations for nearly incompressible flows: Semi-analytic time stepping and absorbing boundary layers. *Journal of Computational Physics*, 390:175–202, August 2019.

[49] A. Karakus, N. Chalmers, J.S. Hesthaven, and T. Warburton. Discontinuous Galerkin discretizations of the Boltzmann–BGK equations for nearly incompressible flows: Semi-analytic time stepping and absorbing boundary layers. *Journal of Computational Physics*, 390:175–202, August 2019.

[50] Torsten Keßler and Sergej Rjasanow. Fully conservative spectral galerkin–petrov method for the inhomogeneous boltzmann equation. *Kinetic & Related Models*, 12(3):507, 2019.

[51] Gerhard Kitzler and Joachim Schöberl. A spatial discontinuous Galerkin method with rescaled velocities for the Boltzmann equation. *arXiv:1903.01904 [cs, math]*, March 2019. arXiv: 1903.01904.

[52] Gerhard Kitzler and Joachim Schöberl. A spatial discontinuous Galerkin method with rescaled velocities for the Boltzmann equation. *arXiv:1903.01904 [cs, math]*, March 2019. arXiv: 1903.01904.

[53] Dana A Knoll and David E Keyes. Jacobian-free newton–krylov methods: a survey of approaches and applications. *Journal of Computational Physics*, 193(2):357–397, 2004.

[54] Julian Koellermeier. Error estimators for adaptive simulation of rarefied gases using hyperbolic moment models. In *AIP Conference Proceedings*, volume 2132, page 120004. AIP Publishing LLC, 2019.

[55] Julian Koellermeier and Marvin Rominger. Analysis and numerical simulation of hyperbolic shallow water moment equations. *Commun. Comput. Phys*, 28(3):1038–1084, 2020.

[56] Julian Koellermeier and Giovanni Samaey. Projective integration schemes for hyperbolic moment equations. *arXiv preprint arXiv:2005.13914*, 2020.

[57] Julian Koellermeier and Ullika Scholz. Spline moment models for the one-dimensional boltzmann–bhatnagar–gross–krook equation. *Physics of Fluids*, 32(10):102009, 2020.

[58] Julian Koellermeier and Manuel Torrilhon. Numerical Study of Partially Conservative Moment Equations in Kinetic Theory. *Communications in Computational Physics*, 21(4):981–1011, April 2017.

[59] Julian Koellermeier and Manuel Torrilhon. Numerical study of partially conservative moment equations in kinetic theory. *Communications in Computational Physics*, 21(4):981–1011, 2017.

[60] Yangyu Kuang and Huazhong Tang. Globally hyperbolic moment model of arbitrary order for one-dimensional special relativistic boltzmann equation. *Journal of Statistical Physics*, 167(5):1303–1353, 2017.

[61] C. David Levermore. Moment closure hierarchies for kinetic theories. *Journal of Statistical Physics*, 83(5-6):1021–1065, June 1996.

[62] Yu Lv. Development of a nonconservative discontinuous galerkin formulation for simulations of unsteady and turbulent flows. *International Journal for Numerical Methods in Fluids*, 92(5):325–346, 2020.

[63] Zhiting Ma. Navier-stokes limit of globally hyperbolic moment equations. *Kinetic & Related Models*, 14(1):175, 2021.

[64] Luc Mieussens. DISCRETE VELOCITY MODEL AND IMPLICIT SCHEME FOR THE BGK EQUATION OF RAREFIED GAS DYNAMICS. *Mathematical Models and Methods in Applied Sciences*, 10(08):1121–1149, November 2000.

[65] Steven Murphy. *Methods for solving discontinuous-Galerkin finite element equations with application to neutron transport.* PhD thesis, 2015.

[66] Anthony T Patera. A spectral element method for fluid dynamics: laminar flow in a channel expansion. *Journal of computational Physics*, 54(3):468–488, 1984.

[67] Per-Olof Persson and Jaime Peraire. Sub-cell shock capturing for discontinuous galerkin methods. In *44th AIAA Aerospace Sciences Meeting and Exhibit*, page 112.

[68] Sandra Pieraccini and Gabriella Puppo. Microscopically implicit–macroscopically explicit schemes for the BGK equation. *Journal of Computational Physics*, 231(2):299–327, January 2012.

[69] Simon Pintarelli. *Deterministic Numerical Methods for the Boltzmann Equation.* PhD thesis, ETH Zurich, 2018.

[70] Gabriella Puppo. Kinetic models of BGK type and their numerical integration. *arXiv:1902.08311 [physics]*, February 2019. arXiv: 1902.08311.

[71] Albert Reuther, Jeremy Kepner, Chansup Byun, Siddharth Samsi, William Arcand, David Bestor, Bill Bergeron, Vijay Gadepally, Michael Houle, Matthew Hubbell, et al. Interactive supercomputing on 40,000 cores for machine learning and data analysis. In *2018 IEEE High Performance extreme Computing Conference (HPEC)*, pages 1–6. IEEE, 2018.

[72] Roman Pascal Schaerer and Manuel Torrilhon. On singular closures for the 5-moment system in kinetic gas theory. *Communications in Computational Physics*, 17(2):371–400, 2015.

[73] Thomas E Schwartzentruber, Leonardo C Scalabrin, and Iain D Boyd. A modular particle–continuum numerical method for hypersonic non-equilibrium gas flows. *Journal of Computational Physics*, 225(1):1159–1174, 2007.

[74] Henning Struchtrup and Manuel Torrilhon. Regularization of grad's 13 moment equations: Derivation and linear analysis. *Physics of Fluids*, 15(9):2668–2680, 2003.

[75] Wei Su, Peng Wang, Yonghao Zhang, and Lei Wu. A high-order hybridizable discontinuous Galerkin method with fast convergence to steady-state solutions of the gas kinetic equation. *Journal of Computational Physics*, 376:973–991, January 2019.

[76] Wei Su, Peng Wang, Yonghao Zhang, and Lei Wu. Implicit Discontinuous Galerkin Method for the Boltzmann Equation. *arXiv:1901.01865 [physics]*, January 2019. arXiv: 1901.01865.

[77] Wei Su, Lianhua Zhu, Peng Wang, Yonghao Zhang, and Lei Wu. Can we find steady-state solutions to multiscale rarefied gas flows within dozens of iterations? *Journal of Computational Physics*, 407:109245, 2020.

[78] Lambert Theisen and Manuel Torrilhon. fenicsr13: A tensorial mixed finite element solver for the linear r13 equations using the fenics computing platform. *ACM Transactions on Mathematical Software (TOMS)*, 47(2):1–29, 2021.

[79] Manuel Torrilhon. Modeling Nonequilibrium Gas Flow Based on Moment Equations. *Annual Review of Fluid Mechanics*, 48(1):429–458, January 2016.

[80] Lloyd N Trefethen and JAC Weideman. The exponentially convergent trapezoidal rule. *siam REVIEW*, 56(3):385–458, 2014.

[81] E.H.S.P.N.G. Wanner, E. Hairer, S.P. Nørsett, mathématicien Gerhard Wanner, and G. Wanner. *Solving Ordinary Differential Equations II: Stiff and Differential-Algebraic Problems*. Solving Ordinary Differential Equations II: Stiff and Differential-algebraic Problems. Springer, 1993.

[82] Armin Westerkamp. *A Continuous Interior Penalty Method for the Linear Regularized 13-Moment Equations describing Rarefied Gas Flows*. PhD thesis, Universitätsbibliothek der RWTH Aachen, 2017.

[83] Tianbai Xiao. A flux reconstruction kinetic scheme for the boltzmann equation. *arXiv preprint arXiv:2103.10371*, 2021.